Study of the Cabibbo-suppressed decay $D^+ \to \pi^+\pi^0\pi^0$

Master thesis

Author	*Student number*
Cristina Sánchez Gras	S2989840

First supervisor: Dr. Myroslav Kavatsyuk

Second supervisor / Referee: Prof. Dr. Olaf Scholten

July 2017

This page is intentionally left blank.

Contents

Chapter 1

Introduction

In the last few decades, the Standard Model (SM) of particle physics has been granted the experimental confirmation of numerous theoretically predicted features, like the observation of the Higgs boson [1], [2] and that of tetraquark states, like the recently discovered $X(4274), X(4500)$ and $X(4700)$ [3]. While the SM has been successful in unifying three of the four fundamental forces and describing the interactions of quarks and leptons at high energies, it still presents some flaws. Satisfactory explanations of these interactions at low energies and the inclusion of the fourth fundamental force are still required. With the purpose of solving the latter, physicists are working on developing a so called "Theory of Everything". The study of charmonium states is particularly appropriate for the understanding of low-energy interactions between quarks. In this chapter, a brief overview of the SM and some of the challenges it faces will be given. In addition, the important role of charmonium in the study of long-distances scales will be presented. Lastly, an explanation of the objective of this master thesis will be provided.

1.1 The Standard Model

The Standard Model (SM) of particle physics is a theory that provides a description of the building blocks of matter (quarks and leptons) and how they interact via three of the four fundamental forces: the strong force, described by Quantum Chromodynamics (QCD), and the electromagnetic and weak forces, unified by the electroweak theory.

The fundamental particles of the SM are shown in Fig. 1.1. In the first three columns, quarks (violet) and leptons (green) are shown. There are six quarks and six leptons, which belong in pairs to three different "generations": the up and down quark form the first generation, the charm and strange one form the second and then the top and bottom quarks conform the third one. Similarly, the e and the ν_e conform the first generation of leptons, the μ and ν_μ the second and the τ and ν_τ the third. Each of these particles has an antiparticle, and all of them have an associated electric charge, being the neutrinos an exception. While leptons can only interact via the electromagnetic and weak forces, quarks can also interact via the strong interaction.

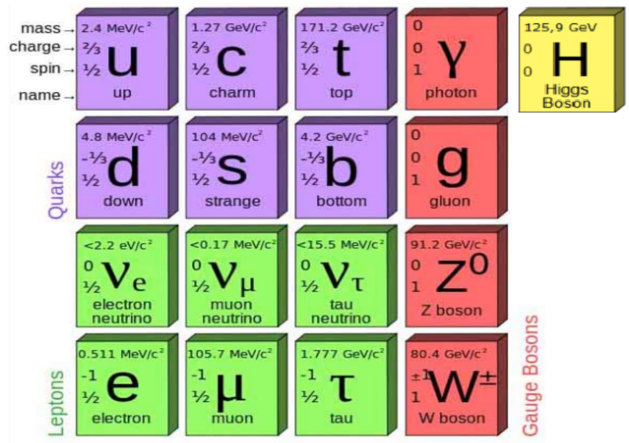

Figure 1.1: The particles of the Standard Model of particle physics. The three generations of quarks and leptons are shown in the first three columns. The forth column contains the gauge bosons that mediate the electromagnetic, strong and weak interactions. The fifth column displays the Higgs boson, a scalar boson.

The electromagnetic, weak and strong forces are mediated by gauge bosons, shown in the fourth column (red) in Fig. 1.1. While the electromagnetic force has an infinite range, the range of the weak and strong forces is very short and they are dominant at subatomic scales. The electromagnetic force is mediated by the photon, γ, which is a massless particle. The gauge bosons of the weak interaction are the heavy $W^{\pm}$ and Z^0 bosons. The gluons are the massless force carriers of the strong interaction. The fifth column shows the Higgs boson, a spin-zero particle that is responsible for the masses of all the elementary particles in the SM. The discovery of the Higgs boson by the ATLAS [1] and CMS [2] experiments in LHC, CERN, [4] was an important breakthrough, as its existence was predicted in 1964 but was first seen in 2012.

Both quarks and gluons carry colour charge, which can be red, green or blue. This is a unique property of the strong interaction that allows for the interaction between quarks and gluons. As mentioned in the beginning of this section, the strong interaction is described by QCD, an SU(3) gauge theory. This force binds quarks and anti-quarks in order to form ”colourless” objects. Baryons, like the proton or the neutron, are formed by three quarks. A quark-antiquark pair forms a meson, such as pions or kaons. Baryons and mesons are well established and are referred to as ordinary matter. Other quark-bound states predicted by QCD, such as tetraquarks, pentaquarks, glueballs or hybrids are called exotic matter. While there have been various observations of states with more than three quarks (for instance see [3]), glueballs and hybrids remain undiscovered.

The strong interaction has two main features: quark confinement and asymptotic freedom. Quark confinement precludes the existence of isolated quarks. As the distance between two quarks gets larger, the interaction between them becomes stronger, and above a certain threshold, a new quark-antiquark pair is created. This phenomenon is what keeps quarks into colourless objects. On the contrary, when the distance between quarks becomes shorter, the interaction between quarks gets weaker. This is known as asymptotic freedom.

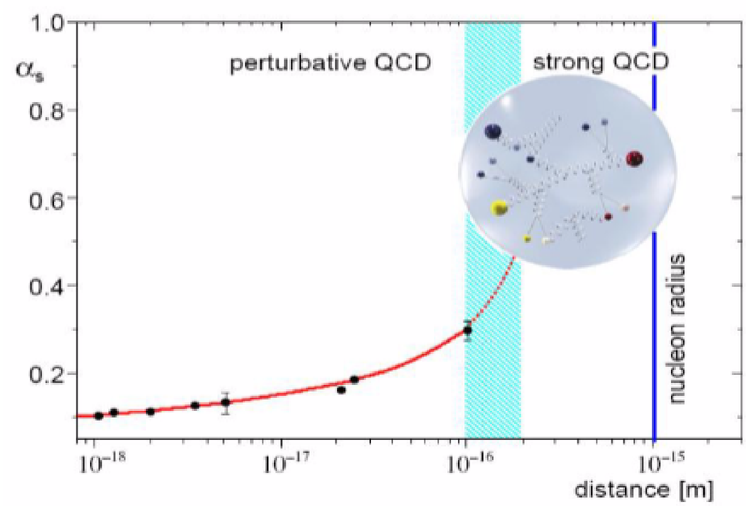

Figure 1.2: Values of the strong coupling constant α_s as a function of the distance between quarks. Charmonium lies on the shaded region of the figure. Taken from [5].

Both quark confinement and asymptotic freedom take place for different regimes of the strong coupling constant, α_s, the expansion parameter in QCD. Its dependence with the distance scale is shown in Fig. 1.2. At short distances (high energies), the value of α_s is small, and perturbative QCD methods can be applied in order to calculate observables. This regime describes asymptotic freedom (short distances). At large distances (low energies), α_s becomes too large and perturbative methods are no longer valid. This is the strong QCD regime, in which non-perturbative methods such as lattice QCD or effective field theories need to be applied. Quark confinement does not have a satisfactory description in the non-perturbative regime of QCD. Understanding the confinement of quarks could lead to the comprehension of the origin of hadron mass, which has its roots in the strong force. For instance, the mass of the proton is about 100 times larger than the mass of their quark components, but the reason behind this phenomenon is still unknown. The spectroscopy of mesons in the charmonium mass region by the BESIII [6] and the future PANDA [7] experiments have the aim of enlightening this mystery. This is done by performing e^+e^- annihilations at center-of-mass energies of $\sqrt{s} = (2 - 4.6)$ GeV for BESIII and $\overline{p}p$ annihilations in PANDA at center-of-mass energies of $\sqrt{s} = (2.5 - 5.5)$ GeV, energies that include the region of charmed bound systems.

1.2 Charmonia spectrum

Charmonium is a meson with a $c\overline{c}$ quark composition. The use of charmonium states for the study of the non-perturbative regime of QCD is favoured due to the mass of the charm quark, $m_c = 1.28 \pm 0.03$ GeV/c^2 (according to the Particle Data Group (PDG) [8]). With such a high mass, the $c\overline{c}$ state can be described my means of a non-relativistic potential that includes spin-orbit and spin-spin corrections. Such a potential must include a Coulomb-like term, to account for the interaction between quarks in the asymptotic freedom regime. In addition, a term with linear dependence on distance must be added to include the quark confinement regime, for which the potential increases with distance. The potential can be modelled as:

$$V(r) = -\frac{4}{3}\frac{\alpha_s(r)}{r} + kr \tag{1.1}$$

where 4/3 accounts for the $c\overline{c}$ required to be in a colour-single state; $\alpha_s(r)$ is the "running" coupling constant (as it depends with the distance r between the quark and anti-quark); and k is a force constant ($k \approx 1$ GeV/fm). The spectrum of charmonium states is shown in Fig. 1.3. Note that those states in yellow are the established $c\overline{c}$ states, and some of them are a consequence of fine-splitting (due to spin-orbit interactions) and hyperfine-splitting (due to spin-spin interactions).

While the grey states are predicted by the theory but yet unobserved, the pink and violet states (neutral and charged XYZ exotic states, respectively) where unpredictably observed. More information about the XYZ states can be found in Section 2.1.1. The line labelled "$2M_D$" in Fig. 1.3 corresponds to the open charm threshold. This is the energy threshold above with charmonium can dissociate into two charmed mesons, i.e., mesons with one c quark and other type of quark. The threshold is equivalent to two times the mass of the lightest charmed meson, the $D^0(c\overline{u})$ with mass $m_{D^0} = 1864.86 \pm 0.05$ MeV/c^2 [8]. The charmonium states above the open charm threshold are expected to primarily decay into $D\overline{D}$ pairs.

Charmonium states with any J^{PC} number can be produced via $p\overline{p}$ annihilations (in experiments such like LHCb [9] in the CERN facility or the future PANDA experiment [7]) or in B-meson decays (in BaBar [10] and Belle [11] at SLAC, for instance). In BESIII, the experiment in which the data used for this work was collected, only 1^{--} charmonium states can be directly produced. This is due to the fact that, in BESIII, e^+e^- annihilations take place in order to create the $c\overline{c}$ states. Since the creation of the $c\overline{c}$ proceeds via a virtual photon, only states with the same quantum numbers that photons can be produced, i.e., 1^{--}. In e^+e^- annihilations, 1^{--} charmonium states can also be produced via the Initial State Radiation (ISR) method, utilised in the CLEO and CLEO-c [12] experiments. In the ISR process, the electron or the positron can emit a photon before annihilation, which lowers the center-of-mass effective energy. The main advantage for charmonium production via e^+e^- collisions instead of $p\overline{p}$ ones is that the hadronic background is considerably smaller with the former method.

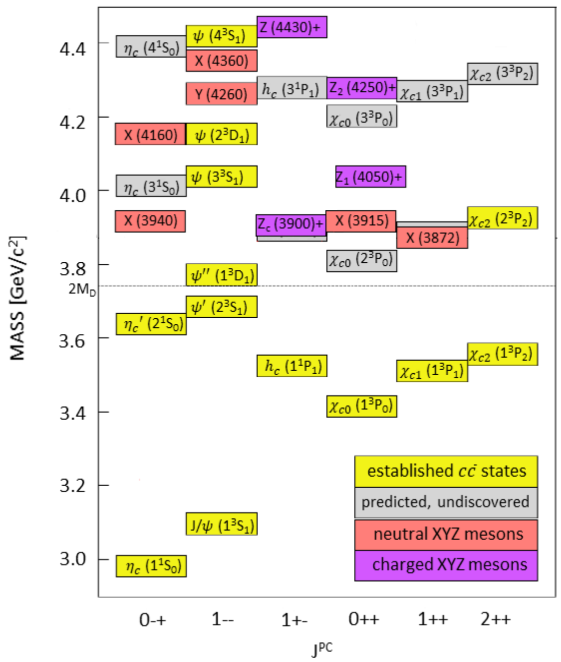

Figure 1.3: Charmonium spectrum. The charmonium states are denoted by the J^{PC} notation in the x-axis, where J stands for total angular momentum, P is the parity of the system and C its charge-conjugation parity.

As discussed in the beginning of the section, charmonium spectroscopy can contribute to the study of the potential that mediates the interaction between quarks. However, that is not the only relevant physics information that can be extracted from this states. They can be utilised in the search for CP violating processes and lepton-flavour violation. Moreover, charmonium is located in the energy region in which exotic states, such as glueballs and hybrids, are expected to be found and, therefore, that characteristic should be exploited. The study of the D charmed mesons, produced in the decays of charmonium states above the $D\overline{D}$ threshold, can provide information about the elements of the quark-mixing matrix. More information about the physics possibilities of charmonium states is given in Section 2.1.

1.3 Objectives

The aim of this master research project is to measure and improve the branching fraction $\mathcal{B}$ of the Cabibbo-suppressed decay $D^+ \to \pi^+\pi^0\pi^0$.

Its current value is $\mathcal{B}(D^+ \to \pi^+\pi^0\pi^0) = (4.5 \pm 0.4) \times 10^{-3}$, and it is based on a measurement performed by the CLEO-c collaboration in 2006 [13]. For that, 281 pb^{-1} of data collected on the ψ'' (also known as $\psi(3770)$) resonance ($\sqrt{s} \approx 3.77$ GeV) with the CLEO-c detector were utilised. The $\psi(3770)$, with mass $m_{\psi''} = (3773.13 \pm 0.35)$ MeV, is the first charmonium state lying above the open charm threshold. It has a large probability of decaying into a pair of D mesons: $\mathcal{B}(\psi'' \to D^0\overline{D^0}) = (52^{+4}_{-5})$ % and $\mathcal{B}(\psi'' \to D^+D^-) = (41 \pm 4)$ %, as stated by the PDG [8], which makes up for a 93% branching ratio for $\psi'' \to D\overline{D}$.

The $\mathcal{B}(D^+ \to \pi^+\pi^0\pi^0)$ result can be improved with the 2917 pb^{-1} of data collected at $\sqrt{s} = 3.773$ GeV by the BESIII collaboration between 2010 and 2011 [14]. These data sets correspond to two different data taken periods: the first part was taken between January and June of 2010 and the second part was taken from December 2010 to May 2011. With these data and the high branching ration for $\psi(3700) \to D^+D^-$, the D^+ mesons can be studied.

What makes interesting the $D^+ \to \pi^+\pi^0\pi^0$ decay is that it is Cabibbo-suppressed. Decays involving quark-flavour mixing can be either (Cabibbo-)favoured or (Cabibbo-)suppressed depending on the flavour mixing that takes place. Favoured decays occur when the matrix element(s) governing the quark-mixing is(are) on the diagonal of the Cabibbo-Kobayashi-Maskawa (CKM) matrix. If the matrix element is off-diagonal, the decay is said to be suppressed (see Section 2.1.2 for more details). As an example, Fig. 1.4 shows the diagrams for the Cabibbo-favoured decay $D^- \to K^+\pi^-\pi^-$ is represented on the right, while the Cabibbo-suppressed decay of interest for this study, $D^+ \to \pi^+\pi^0\pi^0$, is represented on the left. While both diagrams appear to be very similar, the quark-flavour mixing is different for each decay. For the D^- decay, the flavour conversion is $c \to s$, which corresponds to a diagonal element of the CKM matrix. On the contrary, the D^+ decay experiments a $c \to d$ conversion, which is described by an off-diagonal element.

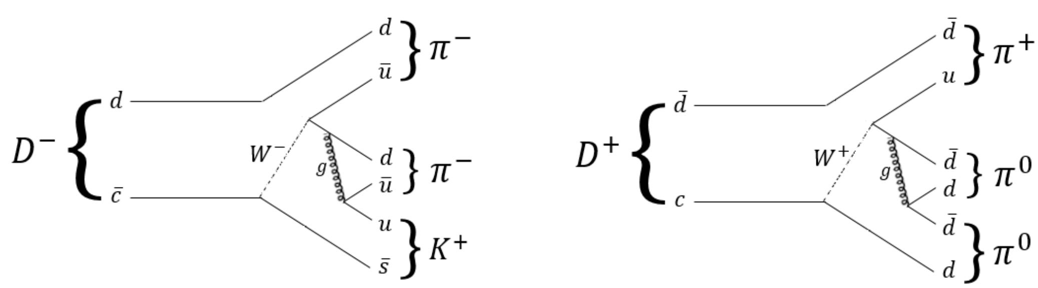

Figure 1.4: Decay diagrams for the Cabibbo-favoured decay $D^- \to K^+\pi^-\pi^-$ (left) and the Cabibbo-suppressed decay $D^+ \to \pi^+\pi^0\pi^0$ (right).

The study of Cabibbo-suppressed D decays remains an interesting field of research. Some of these decays can help in the determination of the γ angle of the CKM matrix. Furthermore, these suppressed decays can be a background for other D decay measurements. Thus, determining their branching fractions become of great importance in order to reduce the background for those analysis more effectively.

The BESIII experiment, its physics program, its detector and its offline sotware will be described in Chapter 2 of this thesis. In Chapter 3, the analysis methods utilised in the data analysis are presented. These include particle identification and reconstruction, kinematic fitting and Monte Carlo (MC) simulations.

Chapter 2

The BESIII experiment

Located at the Institute of High Energy Physics (IHEP) in Beijing, the BESIII (Beijing Electron Spectrometer) experiment [6] was conceived for the study of an extensive physics program, covering charmonium and charm physics, light hadron spectroscopy and τ physics. The experiment is carried out at the Beijing Electron Positron Collider (BEPC)-II, which consists on a two-ring e^+e^- collider. It is designed to operate with a luminosity of $10^{33}\text{cm}^{-2}\text{s}^{-1}$ and beams with center-of-mass energies in the range of $\sqrt{s} = (2-4.6)$ GeV, making it a facility for the study of long-distance scales in QCD with high luminosities. Both BESIII and BEPC-II are the result of an upgrade of their predecessors (the BEPC-I and the BES detector) that took part between 2003 and 2008. Data collection began in March 2009 and the BESIII experiment has gathered the world's largest data samples at charm threshold heretofore. These include $J/\psi, \psi(2S), \psi(3770)$ and the XYZ states.

A summary of the physics goals of the BESIII experiment is given in Section 2.1. The BESIII detector and its offline data software are discussed in Section 2.2

2.1 Physics program of BESIII

The BESIII experiment operates in the energy region $\sqrt{s} = (2-4.6)$ GeV, which corresponds to the frontier between the perturbative and non-perturbative regimes of Quantum Chromodynamics (QCD). The high-energy regime of QCD can be treated perturbatively, since the strong coupling constant, α_s becomes very small. However, in the low-energy regime, α_s becomes too large and the perturbation methods are no longer valid. Therefore, alternative methods such as lattice QCD or effective field theories need to come into play. While the short-distance scales (high-energies regime) are quite well understood, the long-distance scales (low-energies regime) are lacking theoretical and experimental investigation. The BESIII experiment, operating in the energy range between both regimes, aims to enlighten the QCD dynamics for the low-energy regime. Its physics program includes charmonium and light hadron spectroscopy and D and τ physics. A brief summary of these main goals is given in the subsections below. The entire physics program is described in detail in the physics book published by the BESIII collaboration [15].

2.1.1 Charmonium spectroscopy

There are some flagrant challenges arising in charmonium spectroscopy that the BESIII experiment aims to shed light on with high-statistics data sets. One of these notorious problems is the $\rho\pi$ puzzle, or the violations of the 12 %-rule. This rule is based on the assumption that the ratio of the hadronic and leptonic decays of vector charmonium decay branching fractions $\mathcal{B}$ is constant [16]. That ratio can be estimated as follows:

$$R = \frac{\mathcal{B}(\psi' \to \ hadrons)}{\mathcal{B}(J/\psi \to \ hadrons)} = \frac{\mathcal{B}(\psi' \to e^+e^-)}{\mathcal{B}(J/\psi \to e^+e^-)} \tag{2.1}$$

With the values $\mathcal{B}(\psi' \to e^+e^-) = (7.89 \pm 0.17) \times 10^{-3}$ and $\mathcal{B}(J/\psi \to e^+e^-) = (5.971 \pm 0.032)\%$ taken from the Particle Data Group (PDG) [8], it can be calculated that $R = 0.132 \pm 0.003$. This ratio is known as the 12 %-rule (the name was given after former measurements that estimated $R \approx 12\%$). For the 12 %-rule, it is considered that the decays of charmonium states to hadrons via three gluons are dominant. However, this rule is violated for decay channels such as $\rho\pi$ and $K^*\overline{K}$, and none of the theories proposed to explain this behaviour is perfectly solid, which makes it necessary to study charmonium decays in more detail.

A further problem in charmonium spectroscopy are the non-$D\overline{D}$ decays of $\psi(3770)$. The $\psi(3770)$ is the first charmonium state immediately above the open-charm threshold and it is expected to decay primarily to $D\overline{D}$ pairs, in conformity with the OZI rule. Nevertheless, the BES collaboration found a large branching fraction of $\psi(3770)$ decays into non-$D\overline{D}$ pairs, $\mathcal{B}$ ($\psi(3770) \to$ non-$D\overline{D}$) $= (15.1 \pm 5.6 \pm 1.8)\%$ [17]. A later study by the CLEO Collaboration found a value incompatible with that of the BES Collaboration, $\mathcal{B}(\psi(3770) \to$ non-$D\overline{D}) = (3.3 \pm 1.4^{+6.6}_{-4.6})\%$ [18]. These conclusions are inconsistent with the OZI rule, and, together with the disagreement between the results, they indicate that more theoretical and experimental studies are needed.

The BESIII experiment is able to operate at energies above the open-charm threshold. This offers the opportunity of studying the exotic states XYZ. The X states are neutral, the Y states normally have $J^{PC} = 1^{--}$ and can be populated in e^+e^- annihilation experiments such as BESIII; and the Z states are charged states. These states receive the name of "exotic" due to the fact that they have been unpredictably discovered, like for instance the $X(3872)$ [19], the $Y(4260)$ [20] and the $Z_c(3900)^{\pm}$ [21]. More measurements are needed in order to fully comprehend the XYZ states, as well as more accurate theoretical approaches.

2.1.2 D physics

The properties of the charmed mesons D and D_s can be studied with the BESIII experiment. Since the $\psi(3770)$ state decays predominantly to $D\overline{D}$ pairs, the $D^{\pm}$ and D^0 mesons are produced in this manner. The D_s mesons are produced in BESIII with $\sqrt{s} = 4.03$ GeV for the e^+e^- annihilation. By considering purely leptonic decays of these D mesons, the decay constants f_D

and f_{D_s} can be determined. Moreover, the examination of D decays provides the opportunity of measuring the quark-mixing matrix elements, commonly known as the Cabibbo-Kobayashi-Maskawa (CKM) matrix. This matrix has the form:

$$\begin{pmatrix} |V_{ud}| & |V_{us}| & |V_{ub}| \\ |V_{cd}| & |V_{cs}| & |V_{cb}| \\ |V_{td}| & |V_{ts}| & |V_{tb}| \end{pmatrix} = \begin{pmatrix} 0.97417 \pm 0.00021 & 0.2248 \pm 0.0006 & 0.00409 \pm 0.0039 \\ 0.220 \pm 0.005 & 0.995 \pm 0.016 & 0.0405 \pm 0.0015 \\ 0.0082 \pm 0.0006 & 0.0400 \pm 0.0027 & 1.009 \pm 0.031 \end{pmatrix} \tag{2.2}$$

where each $|V_{ij}|^2$ stands for the probability of the i-flavour quark to decay into a j-flavour quark, and their values are given by the PDG [8]. The CKM matrix elements are fundamental parameters of the SM that provide information about the strength of flavour-changing weak decays. In the case of charmed mesons, the c-quark can undergo flavour-mixing. The BESIII experiment can study the decays $D^0 \to K^- e^+ \nu_e$ and $D^0 \to \pi^- e^+ \nu_e$ in order to measure the V_{cs} and V_{cd} respectively.

Furthermore, BESIII will be able to study $D - \overline{D}$ oscillations in order to search for CP-violating processes and to perform a precision measurement of the CKM mixing angle γ [22]. Some of the relations of the CKM matrix can be expressed graphically as triangles in the complex plane, and while there is a measurement for the β angle and a constraint on the α angle, there is no satisfactory measurement of the γ angle.

Cabibbo-suppressed decay channels of D mesons can be studied in detail with the large data samples of BESIII. The CKM matrix diagonal elements are near unity, whereas the off-diagonal elements are small. Those decays that are mediated by a diagonal element, i.e. $c \to s$ in $D^- \to K^+ \pi^- \pi^-$ are said to be Cabibbo-favoured; but those mediated by an off-diagonal element, such as the $c \to d$ mixing taking place in $D^+ \to \pi^+ \pi^0 \pi^0$ are Cabibbo-suppressed. The study of these decay channels, together with the study of rare or forbidden decays of D mesons can reveal new physics beyond the SM.

2.1.3 Light hadron spectroscopy

The energy range of the BESIII experiment allows the search for glueballs and the spectroscopy of light hadrons in order to determine their gluon content. The existence of glueballs and their masses are predicted by the SM. In BESIII, J/ψ decays will be used in this search, since the $c\bar{c}$ quarks forming the J/ψ have a large probability of annihilating into gluons. Moreover, a study of SM predicted exotic hadrons, such as four-quark states, can be done with the large data samples of BESIII.

2.1.4 τ physics

The τ, with a mass of about 1.77 GeV/c^2, is the only lepton that can decay into hadrons. By studying inclusive hadronic decays, the CKM matrix element V_{us} can be determined. These leptons can be produced in BESIII at the production threshold of 3.55 GeV. In 2014, the BESIII Collaboration was able to improve the measurement of the mass of the τ lepton [23]. In addition, the study of their leptonic decays can probe the universality of the electroweak interaction, and possibly hint physics beyond the SM.

2.2 The BESIII Detector

In order to achieve the previously stated physics goals, the BESIII experiment requires a state-of-the-art detector, depicted in Fig. 2.1. The BESIII detector has a solid angle coverage of $\Delta\Omega/4\pi = 0.93$ and a polar angle coverage of $21° < \theta < 159°$ [24], [25]. Its detector parameters are summarised in Table 2.1. The detector is comprised by four main sub-detectors, with the three innermost ones embedded in a 1 T superconducting solenoid magnet. These sub-detectors are:

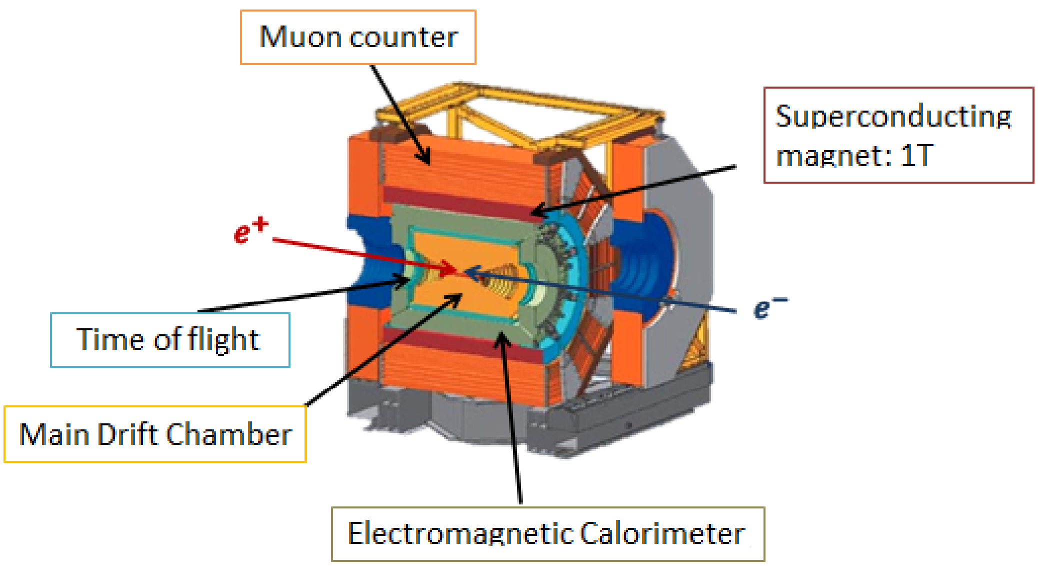

Figure 2.1: Schematics of the BESIII detector.

- A Multilayer Drift Chamber (MDC) that surrounds the beryllium beam pipe, and is filled with a gas mixture of 60 % helium and 40 % propane. The inner radius of the MDC is 59 mm and the outer one is 810 mm. Its function is to resolve the momentum and position of relatively low momentum particles and to produce trigger signals on the first trigger level (trigger details explained later) in order to reject background events.

- A Time-Of-Flight (TOF) system, counting with two layers of 88 plastic scintillator bars each. It is formed by a barrel and two end caps. The efficient time resolution of the TOF grants a 3σ π/K separation up to 700 MeV/c at 90°. Its duty is to measure the time that charged particles use for travelling from the interaction point to the TOF in order to identify their nature. Moreover, it also has an important role in the rejection of background.

- An Electromagnetic Calorimeter (EMC) built from 6240 CsI(Tl) scintillating crystals. The EMC can measure with the energies of photons with energies above 20 MeV with a high precision. In addition, it has an outstanding capability to distinguish e/π for momentum higher than 200 MeV/c. Its aim is to determine the energy and position of charged and neutral particles.

- A Muon Detector (MD), situated outside of the solenoid magnet and formed by resistive plate counters. The goal of the MD is to separate muons from hadrons and background. This separation becomes competent for momentum around 0.4 GeV/c.

Solenoid magnetic field	1 T
Solid angle coverage $\Delta\Omega/4\pi$	93 %
Polar angle coverage θ	$21° < \theta < 159°$
MD (Muon Detector)	
Number of layers in barrel	9
Number of layers in end cap	8
Cut-off momentum:	0.4 MeV/c
EMC (Electromagnetc Calorimeter)	
Energy resolution barrel σ_E/E	< 2.5 % at 1 GeV
Polar angle coverage barrel	$\lvert\cos\theta\rvert < 0.82$
Energy resolution end cap σ_E/E	< 5 % at 1 GeV
Polar angle coverage end cap	$0.83 < \lvert\cos\theta\rvert < 0.93$
Spatial resolution $\sigma_{x,y}$	6 mm at 1 GeV
TOF (Time-Of-Flight)	
Time resolution barrel σ_T	100 ps
Polar angle coverage barrel	$\lvert\cos\theta\rvert < 0.83$
Time resolution end cap σ_T	110 ps
Polar angle coverage end cap	$0.85 < \lvert\cos\theta\rvert < 0.95$
MDC (Mutilayer Drift Chamber)	
Spatial resolution single wire $\sigma_{r\phi}$	130 μm
Momentum resolution σ_p/p	0.5 % at 1 GeV

Table 2.1: Parameters of the subdetectors in BESIII. Further details are described in [24] and [25].

The trigger and data acquisition systems of the BESIII detector are designed with the aim of suppressing background events against good ones. Since the detector faces a high event and background rate, it is necessary that large amounts of data are processed in real time. The trigger system is divided in two levels. At the Level 1 (L1), the trigger signals generated by the MDC, TOF and EMC are processed in order to obtain hit counts in the MDC and TOF and cluster counts in the EMC. The Level 3 (L3) trigger is a software trigger that involves event building and filtering so that the selected good events are stored.

2.2.1 BOSS: BESIII Offline Software System

The BESIII Offline Software System (BOSS) [26] conforms the software framework for data-processing and physics analysis. It is developed in C++ programming language within the Scientific Linux operating system modelled by CERN. BOSS includes external high energy physics libraries such as CERNLIB [27], CLHEP [28], ROOT [29] and Geant4 [30]. The software is composed of five parts: a general framework, simulation, calibration, reconstruction and analysis tools.

There are three types of event data defined in the BOSS framework: raw data, reconstructed data and Data-Summary-Type (DST) data; the last two provided in ROOT format. In the DST files, the reconstructed data is stored for further physics analyses. The simulation part is governed by the BESIII Object Oriented Simulation Tool (BOOST) [31], based on Geant4, which is used to create the detector geometries. The event generators belonging to this part will be discussed in Section 2.2.2. The calibration software provides reconstruction algorithms to obtain calibration data items. The reconstruction package incorporates reconstruction algorithms, such as the MDC tracking algorithm, the dE/dx and TOF reconstruction algorithms, an EMC clustering and shower finding algorithm and a muon track finder. Lastly, in the analysis tools part, the analysis object builder collects the reconstruction results in order to build data items that are suitable for physics analysis. The tools involved include Particle IDentification (PID) and kinematic fitting.

2.2.2 Event generators

Event generators are indispensable in experimental physics in order to maintain the systematic uncertainties to a minimum. Since they can be used for studying detection efficiencies and backgrounds, Monte Carlo (MC) simulations are utilised for that purpose. The MC simulations are expected to be in good agreement with the data, and every dissimilarity is included as systematic errors in the final outcome. In BESIII, the event generator framework for charmonium decays is KKMC+BestEvtGen [32].

The KKMC event generator [33] is designed for the processes $e^+e^- \to f\overline{f} + n\gamma$, where $f = \mu, \tau, u, d, c, s, b$. It is utilised to simulation of $c\overline{c}$ via e^+e^- annihilations. Its most important feature is that it includes Initial State Radiation (ISR) and Final State Radiation (FSR) corrections calculated in QED up to second order. This characteristic is of extreme importance for the incorporation of ISR effects in the generation of charmonium states, such as

$J/\psi, \psi(2S), \psi(3770), \psi(4030), \psi(4160), \psi(4415)$ and lower-lying resonances such as $\rho, \rho', \rho'', \omega, \omega', \phi, \phi'$.

The BestEvtGen is an event generator developed from EvtGen [34]. Its function within the BESIII generator framework is to simulate the various decays of the charmonium states, $c\bar{c} \to X$. There are many different decay models implemented in BestEvtGen, like VLL (decay of vector to two leptons), SLN (decay of scalar to lepton and neutrino) and JPE (decay of vector to photon and pseudoscalar). In the case treated in this thesis, the decay model PHSP is utilised in order to generate decays according to phase-space for the following decays: $\psi(3770) \to D^+D^-,\ D^- \to K^+\pi^-\pi^-,\ D^+ \to \pi^+\pi^0\pi^0,\ \pi^0 \to \gamma\gamma$.

Chapter 3

Analysis Methodology

The objective of the work presented in this thesis is to measure and improve the branching fraction $\mathcal{B}(D^+ \to \pi^+\pi^0\pi^0)$. The method followed to calculate such a result, together with the different reconstruction techniques used in the data analyses are described in this chapter.

3.1 D^+ selection

The BESIII data utilised for the analysis correspond to two data sets collected at the center-of-mass energy of the ψ'' charmonium state. This state is characterised by a large probability of decaying into a D^-D^+ pair (about 40 %). The analysis procedure involved in this thesis is based on the fact that D^+ mesons are produced in pairs with D^- mesons.

The branching ratio of the $D^+ \to \pi^+\pi^0\pi^0$ decay can be calculated as the ratio between the number of D^+ mesons that decay via that particular channel and all the D^+ mesons produced in the $\psi'' \to D^+D^-$ decay. Taking into account that $\mathcal{B}(D^+ \to \pi^+\pi^0\pi^0) = (4.5 \pm 0.4) \times 10^{-3}$ [8] is very small and that D^+D^- are produced in pairs, the D^+ selection procedure is as follows:

1. A D^- decay channel with a relatively high branching fraction is selected. In the case of this thesis, $D^- \to K^+\pi^-\pi^-$, with a branching fraction $\mathcal{B}(D^- \to K^+\pi^-\pi^-) = (8.98 \pm 0.28)$ % [8] is selected.
2. The D^- mesons are reconstructed. Since they are produced in pairs with D^+ mesons, the number of D^+ mesons created together with the D^- decaying via the aforementioned channel, $N_{totalD^+produced}$, is known.
3. The D^+ mesons are reconstructed from the decay products of the channel of interest: π^+ and $2\pi^0$. Then, the number of D^+ mesons decaying via that channel, $N_{D^+\to\pi^+\pi^0\pi^0}$ is known.

4. The branching fraction can be calculated as:

$$\mathcal{B}(D^+ \to \pi^+\pi^0\pi^0) = \frac{N_{sig}^{D^+}}{N_{sig}^{D^-} \cdot \epsilon_{D^+} \cdot \mathcal{B}(\pi^0 \to \gamma\gamma) \cdot \mathcal{B}(\pi^0 \to \gamma\gamma)} \tag{3.1}$$

where $N_{sig}^{D^+}$ is the number of signal events for D^+, $N_{sig}^{D^-}$ is the number of signal events for D^- and ϵ_{D^+} is the D^+ detection efficiency, assuming that π^0 decays exclusively to $\gamma\gamma$. The branching fraction $\mathcal{B}(\pi^0 \to \gamma\gamma)$ needs to be included twice in the calculation to account for the probability that both π^0 actually decay into two photons each. Its value, according to the PDG, is $\mathcal{B}(\pi^0 \to \gamma\gamma) = (98.823 \pm 0.034)\%$ [8].

The D^+ selection procedure is summarised in Fig. 3.1. The π^0 mesons will be reconstructed from a $\gamma\gamma$ pair, since their mean life is too short (about 10^{-16} s) and $\mathcal{B}(\pi^0 \to \gamma\gamma) = (98.823 \pm 0.034)$ % [8]. Events are selected if at least one K^+ and two π^- are present. Thus, the D^+ reconstruction is based on the reconstruction and identification of $D^- \to K^+\pi^-\pi^-$.

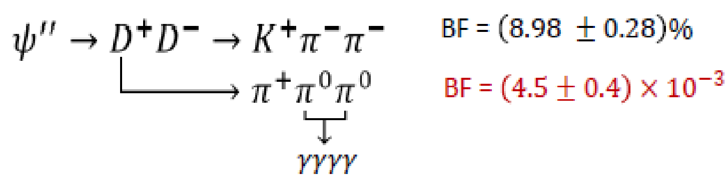

Figure 3.1: Decay modes reconstructed in the analysis presented in this thesis. On the right, the branching fractions (BF) given by the PDG [8] for the $D^- \to K^+\pi^-\pi^-$ decay (top, black) and for $D^+ \to \pi^+\pi^0\pi^0$ (bottom, red).

3.2 Event reconstruction

In this section, the methods used for particle identification (PID) and event reconstruction in this work, together with the event selection criteria determined by BESIII are described. The section is based on information provided by the BESIII physics book [15].

3.2.1 Identification and reconstruction of tracks

PID conforms an essential step in physics analyses. Every part of the BESIII detector plays a role in the particle identification process. However, each sub-detector behaves differently regarding PID for different momentum ranges. Due to that, the strategy followed in order to improve PID is the combination of information from different sub-detectors.

The identification and reconstruction of pions and kaons can be performed in a rather simple way. For that, the momentum information collected by the MDC is utilised. If the momentum of a certain particle is smaller than 1.40 GeV/c, the particles are identified as π/K. If larger, they are identified as leptons, which are not relevant in this work.

With the aim of discerning between pions and kaons, the information of the MDC is combined with the energy loss dE/dx and the TOF data. The energy loss dE/dx of a charged particle is dependent on the ratio m/p, where m is the mass of the particle and p its momentum. By measuring dE/dx, a distinction between π/K can be made. The information of the TOF is used to improve this distinction. The TOF stores the time that a charged particle travels between the interaction point and the TOF detector. With this and the momentum information, the mass of the particle can be determined. The TOF can provide a 2σ π/K separation for momentums up to 900 MeV/c, while the dE/dx information can achieve a 3σ π/K separation for momentum below 600 MeV/c [15]. The combination of these data is utilised to perform a hypothesis test in order to determine if the particle is a kaon or a pion. The PID information is assigned to the candidate with a higher confidence level.

In order to distinguish good charged-track candidates of interest for the considered process from background events, pions and kaons are required to satisfy:

- Tracks must be contained within $|\cos\theta| < 0.93$ of the MDC.
- The distance between the interaction point ant the reconstructed vertex point must be $V_{xy} < 1$ cm in the transverse plane and $V_z < 10$ cm in the beam direction.
- The momentum of reconstructed tracks in the MDC is required to be $p < 2.0$ GeV/c.

Photons are reconstructed from electromagnetic shower clusters in the EMC. An electromagnetic shower started by a photon normally takes place via e^+e^- production. Since the background for this identification is too large due to bremsstrahlung photons and other showers, the photon candidates are required to:

- Have an angle larger than 10° between the photon and the closest charged track.
- The energy deposited in the EMC must be larger than 25 MeV in the barrel and larger than 50 MeV in the end caps.

3.2.2 Kinematic fitting

An additional tool for the reconstruction of particles is kinematic fitting. This procedure consists on making use the physics behind a particle interaction or decay in order to increase the precision of the measurements that describe the event of interest. The physics information is provided via constraints, requiring that measured and non-measured magnitudes fulfil specific kinematic constraints, such as mass invariance of particles or energy and momentum conservation. The kinematic fit is performed by incorporating the constraints via Lagrange multipliers in a least-square fitting procedure. In this fit, the measured values are changed within their uncertainties in order to fulfil the constraints. As a result, the χ^2 of the fit is obtained, which can be utilised for the removal of background and, therefore, the improvement of the signal-to-background ratio.

In this work, a one-constraint (1C) kinematic fit is used for the reconstruction of π^0. The constraint requires that the mass of a $\gamma\gamma$ pair is equal to the mass of the π^0. The results of kinematic fitting for the π^0 reconstruction are discussed in Chapter 4.

3.3 Detection efficiency

The determination of the detection efficiency ϵ is required in order to normalise the number of detected particles. For that, dedicated MC simulations are performed. The detection efficiency does not only depend on the reconstruction algorithm but also on the particle type. For instance, while π/K can be reconstructed with a fairly good ϵ, the same does not happen for photons, since the EMC energy and momentum determination is quite lousy.

Exclusive MC simulations contemplating only the decay channels of interest are executed. In that way, background from other decay channels of D^+ are suppressed. The detection efficiency ϵ is defined as:

$$\epsilon = \frac{n}{N} \tag{3.2}$$

where N is the total number of generated MC events and n the number of detected events after reconstruction.

This definition for ϵ can only be employed if the MC simulations are in accordance with those of data. Some events fail to pass the selection cuts in the detection and reconstruction algorithms for different reasons, like events that do no fire a trigger signal or inefficient reconstruction algorithms. Therefore, the reliability of the MC results must be high in order to trust its outcome.

In the work presented in this thesis, the detection efficiency of the decay channel $D^+ \to \pi^+\pi^0\pi^0$ is calculated. For that, an exclusive MC with the following chosen branching fractions:

- $\mathcal{B}(\psi(3770) \to D^+D^-) = 100\%$
- $\mathcal{B}(D^+ \to \pi^+\pi^0\pi^0) = 100\%$
- $\mathcal{B}(\pi^0 \to \gamma\gamma) = 100\%$
- $\mathcal{B}(D^- \to K^+\pi^-\pi^-) = (8.98 \pm 0.28)\%$, value taken from the PDG [8].

3.4 Input-output check

The input-output check is performed for the purpose of inspecting if the operation of the analysis methods are suitable. In order to do so, the event selection and reconstruction requirements utilised in data are also applied to an inclusive MC sample.

The difference between inclusive MC and exclusive MC simulations is that, in the former, all possible decays for each of the particles involved in every event are taken into account. Thus, $\psi(3770)$ is not constrained to always decay into D^+D^-, and in the same manner, D^+ is not only considered to decay into $D^+ \to \pi^+\pi^0\pi^0$ and π^0 does not only decays into $\gamma\gamma$. This leads to a MC sample that includes all kinds of background decay channels for the decay channel of interest, resembling a collected real data sample. The branching fractions for each decay are those published by the PDG [8].

The analysis procedure used for data is also applied to the inclusive MC sample. In the case treated in this thesis, the branching fraction of $D^+ \to \pi^+\pi^0\pi^0$ is obtained from the inclusive MC results and compare to the data calculations. If the analysis method is proper, the results for data are in good agreement with those of inclusive MC. Generally, if the difference between data and inclusive MC results is within 2σ, the analysis method is considered to be competent.

Chapter 4

Analysis of $D^+ \to \pi^+\pi^0\pi^0$ with 2010 data from BESIII at $\sqrt{s} = 3.773$ GeV

In this chapter, the event analysis for the calculation of $\mathcal{B}(D^+ \to K^+\pi^-\pi^-)$ with BESIII data collected at $\sqrt{s} = 3.773$ GeV in 2010 is shown. The process starts with the reconstruction of D^- via its decay into $K^+\pi^-\pi^-$. Subsequently, the reconstruction of π^0 takes place, and after that the D^+ events of interest are built. The branching fraction calculation is performed in both data and an inclusive MC sample in order to test the validity of the analysis procedure. Two different analysis are presented in Sections 4.1 and 4.2: one based in invariant mass reconstruction of the D mesons via their decay products, and another one based on the usage of two kinematic variables, $\Delta E = E_{beam} - E_D$ and $M_{bc} = \sqrt{E_{beam}^2 - \mathbf{p}_D^2}$, where E_{beam} is the beam energy and E_D, $\mathbf{p}_D^2$ are the energy and momentum of the D candidate.

The analysis in this chapter is made on data collected by BESIII at the ψ'' resonance. The data collection took place from January 2010 to June 2010 with an integrated luminosity of $(927.67 \pm 0.10 \pm 9.28)$ pb^{-1} [14], where the first error is statistical and the second systematic. Defining the total number of $\psi(3770)$ events is not straightforward due to the broad width of the resonance. However, the number of D^+D^- events, N, can be determined with the integrated luminosity, $\mathcal{L}$, and the D^+D^- cross-section at $\sqrt{s} = 3.773$ GeV, $\sigma = (2.830 \pm 0.011(stat.) \pm 0.026(sys.))$ nb [35] via the relationship $N = \sigma\mathcal{L}$. The total number of D^+D^- events is calculated to be $(26.25 \pm 0.10) \cdot 10^5$, where the error is statistical.

An exclusive MC simulation with $50 \cdot 10^3$ samples is utilised in order to determine the detection efficiency and the signal shape. The sample is generated with the event generator framework in BESIII for charmonium decays, KKMC+BestEvtGen, which is described in Section 2.2.2. In the same way, an inclusive MC data sample based on $290 \cdot 10^5$ $\psi(3770)$ decays is used to perform an input-output check as described in Section 3.4.

The data reconstruction and the generation of the MC samples was handled by the BESIII Offline Software System (BOSS) (version 6.6.4), which is described in 2.2.1. The data analysis is done by means of the ROOT [29] software, including the ROOFIT library.

The $D^+ \to \pi^+\pi^0\pi^0$ event selection is described in Sections 3.1 and 3.2. Since the D^+ candidates are reconstructed taking into account the $D^- \to K^+\pi^-\pi^-$ reconstruction, events are kept for further analysis if at least one K^+ and two π^- are present.

4.1 Invariant mass reconstruction of $D^{\pm}$

4.1.1 D^- reconstruction

The decay channel considered for the reconstruction of D^- is $D^- \to K^+\pi^-\pi^-$. The decay products are identified via the combination of information from the TOF, MDC and the energy loss, dE/dx. A hypothesis test is performed in order to distinguish between K/π. If the probability of the track being a K is larger than that of being a π, i.e., $P(K) > P(\pi)$, with $P(K), P(\pi) > 0$, then the track is assigned to a kaon and vice versa.

The invariant mass distribution of $K^+\pi^-\pi^-$, $M_{K^+\pi^-\pi^-}$, reconstructed for each event is shown in Fig. 4.1.

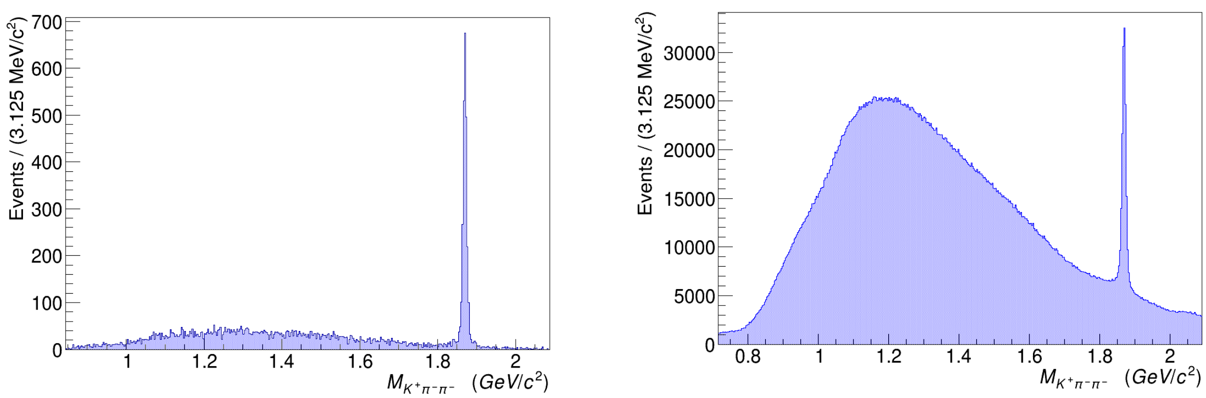

Figure 4.1: Invariant mass distribution $M_{K^+\pi^-\pi^-}$ for the exclusive MC sample (left) and the data set (right).

It can be observed that there is a large combinatorial background for data, but there is no other resonance appearing than that at approximately the D^- mass, which is $M_{D^{\pm}} = (1869.59 \pm 0.09)$ MeV/c^2, according to the PDG [8]. The resonance peak is sharp and narrow. The event reconstruction efficiency is given by the exclusive MC simulation as described in Section 3.3, and it is calculated to be $(61.76 \pm 0.01)\%$ (the error is statistical). This is a value that fits within the expected efficiency for a purely hadronic decay.

The number of $D^- \to K^+\pi^-\pi^-$ signal events can be extracted by fitting the resonance peak. The fitting results are shown in Fig. 4.2. The signal line shape is taken as a non-relativistic Breit-Wigner function, which is used to model resonance shapes. The combinatorial background is fitted via a second-order Chebyshev polynomial function, where its coefficients are free parameters of the fit. The total fit is of the signal and background is given by a probability density function (PDF) described by the sum of the signal line shape and the background.

The resonance takes place at a mass of (1869.15 ± 0.02) MeV/c^2. The signal yield extracted after the fit is of 150071 ± 1194 $D^- \to K^+\pi^-\pi^-$ events.

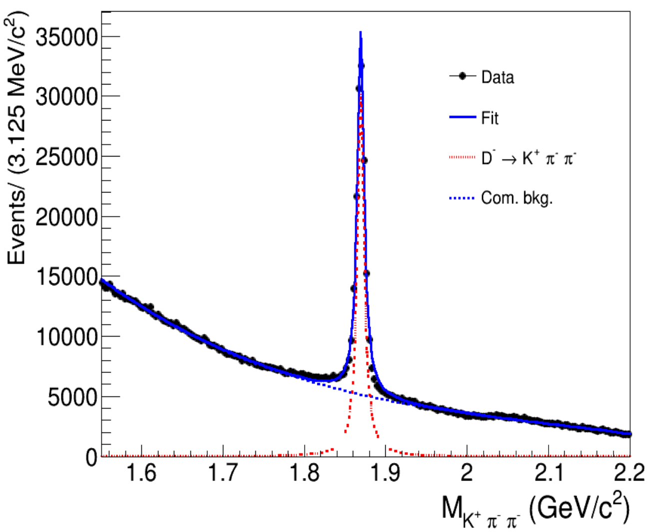

Figure 4.2: Fit result for the invariant mass distribution $M_{K^+\pi^-\pi^-}$ that corresponds to the channel $D^- \to K^+\pi^-\pi^-$. The dots represent data, the solid (blue) line represents the total fit, the dotted red line represents the signal fit and the dashed blue line represents the combinatorial background.

4.1.2 π^0 reconstruction

In order to build D^+ from the decay products in the channel of interest for this thesis, π^0, with mass $M_{\pi^0} = (134.9770 \pm 0.0005)$ MeV/c^2 (PDG [8]) need to be identified. π^0 are reconstructed via their decay into two photons, which happens with a probability of $(98.823 \pm 0.034)\%$ (PDG value [8]. The photon multiplicity distributions for exclusive MC and data are shown in Fig. 4.3.

In principle, the events of interest for this analysis are those with $N_\gamma = 4$, since there are two π^0 involved in the decay channel. Nevertheless, bremsstrahlung photons, together with other showers, result in events with more photons for the observed channel. The photon multiplicity

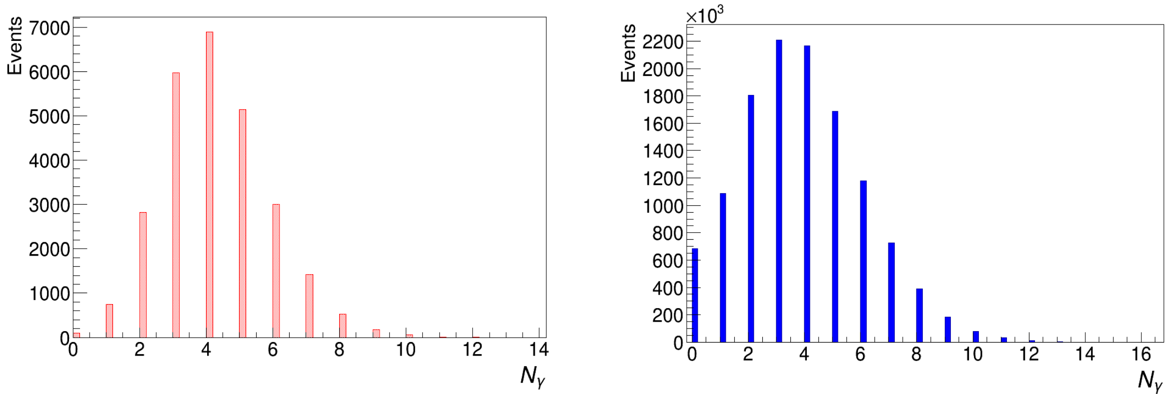

Figure 4.3: The photon multiplicity N_γ per event for the exclusive MC simulation (left, red) and data (right, blue).

distributions look very similar for exclusive MC and data. Possible differences between the MC simulation and data may have their origin in a large background from other decays having greater N_γ in data.

The π^0 candidates are reconstructed via two different ways: by performing an invariant mass reconstruction of them with two γ, and by executing a 1C kinematic fit in which the mass of a pair of photons is required to be equal to that of the π^0 resonance.

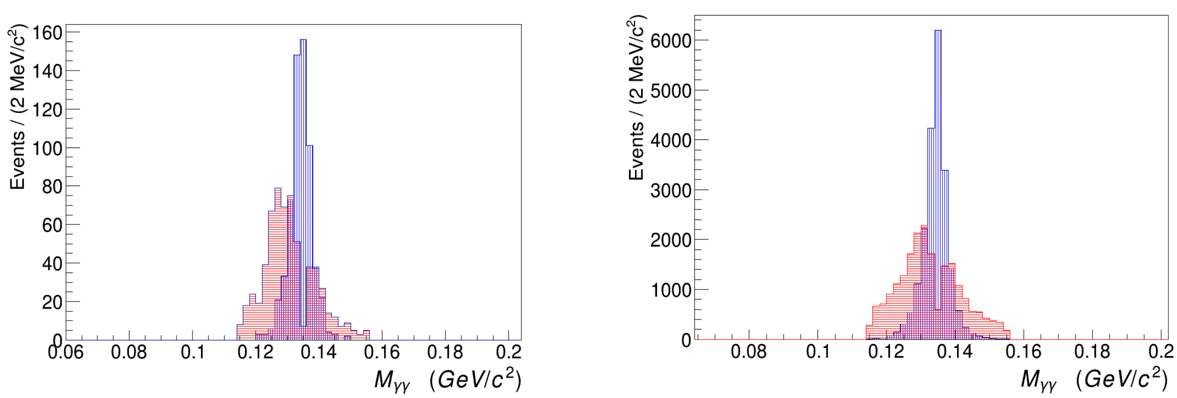

Figure 4.4: Invariant mass distribution $M_{\gamma\gamma}$ for the exclusive MC sample (left) and the data set (right). The curve filled with blue vertical lines represents the first reconstructed π^0 via invariant mass reconstruction and the second one is represented by the curve filled with red horizontal lines.

The results for the first method, π^0 invariant mass reconstruction, for exclusive MC and data are shown in Fig. 4.4. It is required that the event has $N_\gamma \geq 4$ in order to proceed with the π^0 invariant mass reconstruction. Moreover, the mass of the photon pair is required to be $0.115 < M_{\gamma\gamma}$ (GeV/c^2) < 0.155. For the reconstruction, up to 14 photons per event are stored, and then combined in order to obtain the π^0. The curve filled with blue vertical lines in the figure represents the first reconstructed π^0, while the one filled with red horizontal lines represents the second one. The results for MC resemble those for data. It is clear that the reconstruction of the second π^0 is not as neat as for the first one. The reason behind it is that the best combination of photons is taken to reconstruct the first π^0, and the second best combination is utilised for the reconstruction of the second π^0. Therefore, the second one is intrisically built in a worse manner.

Fig. 4.5 shows the results for the reconstruction of both π^0 via kinematic fitting. The mass spectrum shown in the figure corresponds to events where D^+ was identified. In this case, it is required that $2 \leq N_\gamma \leq 4$ and $0.11 < M_{\gamma\gamma}$ (GeV/c^2) < 0.16. It is seen that the first reconstructed π^0 is observed very clearly, but contrary to the results for the previous method shown in Fig. 4.4, the second reconstructed π^0 for the decay $D^+ \to \pi^+\pi^0\pi^0$ is notably improved with respect to the former method. This improvement of the reconstruction of both π^0 is specially well observed on the data results. Further studies on how these two methods work for the D^+ reconstruction via the $D^+ \to \pi^+\pi^0\pi^0$ decay are shown in the following section.

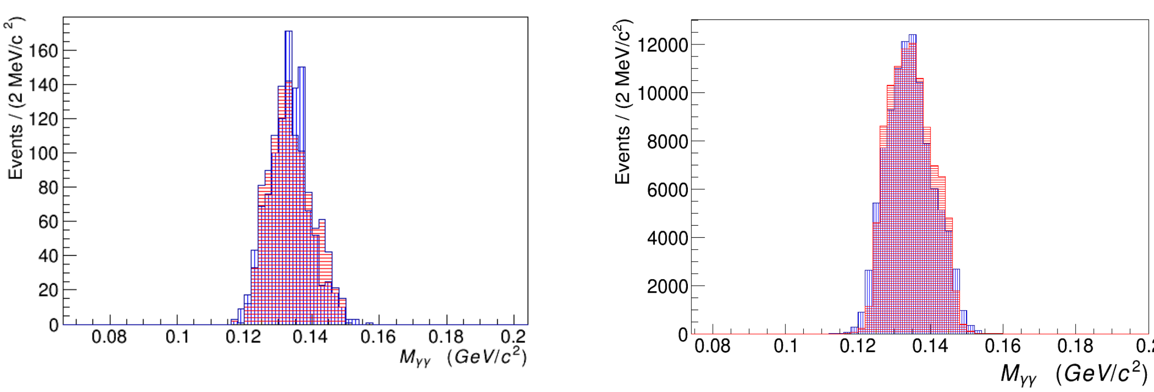

Figure 4.5: Invariant mass distribution $M_{\gamma\gamma}$ for the exclusive MC sample (left) and the data set (right) after kinematic fitting for the reconstruction of π^0. The curve filled with blue vertical lines represents the first reconstructed π^0 and the second one is represented by the curve filled with red horizontal lines.

4.1.3 D^+ reconstruction

The D^+ candidates are reconstructed from the decay channel $D^+ \to \pi^+\pi^0\pi^0$. The pion is identified via the prodecure described in Section 3.2, whereas the π^0 candidates are reconstructed from a pair of photons in the two ways described in the previous section. In this section, the results for the D^+ reconstruction considering both methods for π^0 identification are shown.

When including the results from the kinematic fitting for π^0, the value of the goodness-of-fit, χ^2_{KF}, is taken into account. A cut-off value for the χ^2_{KF} is chosen with the aim of maximising the signal-to-background ratio. The magnitude of χ^2_{KF} serves as an indicator of how proper the fitting procedure is. Therefore, data events with a large χ^2_{KF} compared to the χ^2_{KF} of exclusive MC results are eliminated to improve the signal-to-background ratio. This is done by plotting the statistical significance $N_{sig}/\sqrt{N_{sig}+N_{bkg}}$ against different values of χ^2_{KF}, where $N_{sig}(N_{bkg})$ is the number of signal (background) events obtained with exclusive MC samples. This plot is shown in Fig. 4.6. The fluctuations in the curve show that the method is quite sensitive to statistical fluctuations. In this case, the cut-off value chosen is $\chi^2_{KF} < 16$.

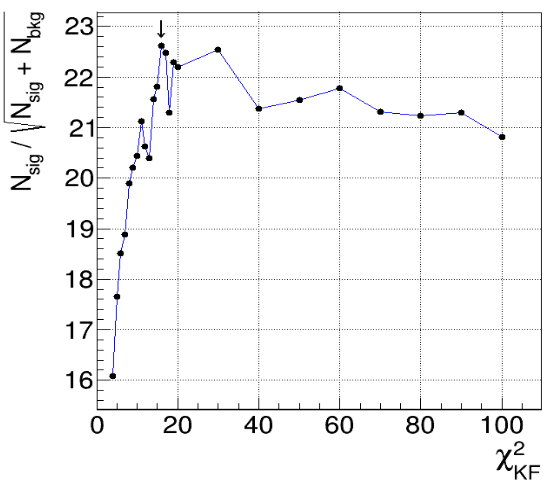

Figure 4.6: Statistical significance $N_{sig}/\sqrt{N_{sig}+N_{bkg}}$ versus different χ^2_{KF} values, where KF stands for kinematic fitting. A cut on $\chi^2_{KF} < 16$ was chosen, indicated with an arrow on the plot.

The invariant mass distribution $M_{\pi^+\gamma\gamma\gamma\gamma}$ is shown in Fig. 4.7. In the first row, the exclusive MC results and the data ones for the case in which π^0 are a product of an invariant mass reconstruction with two γ (from here on, first reconstruction method for π^0) are plotted. The distributions in the second row represent exclusive MC and data results for the π^0 reconstruction via kinematic fitting (from here on, second reconstruction method for π^0. It is observed that the combinatorial background in data is much larger when kinematic fitting is used than when it is not. Moreover, the signal peak for D^+ is much dimmer for the case in which kinematic fitting is used than when it is not.

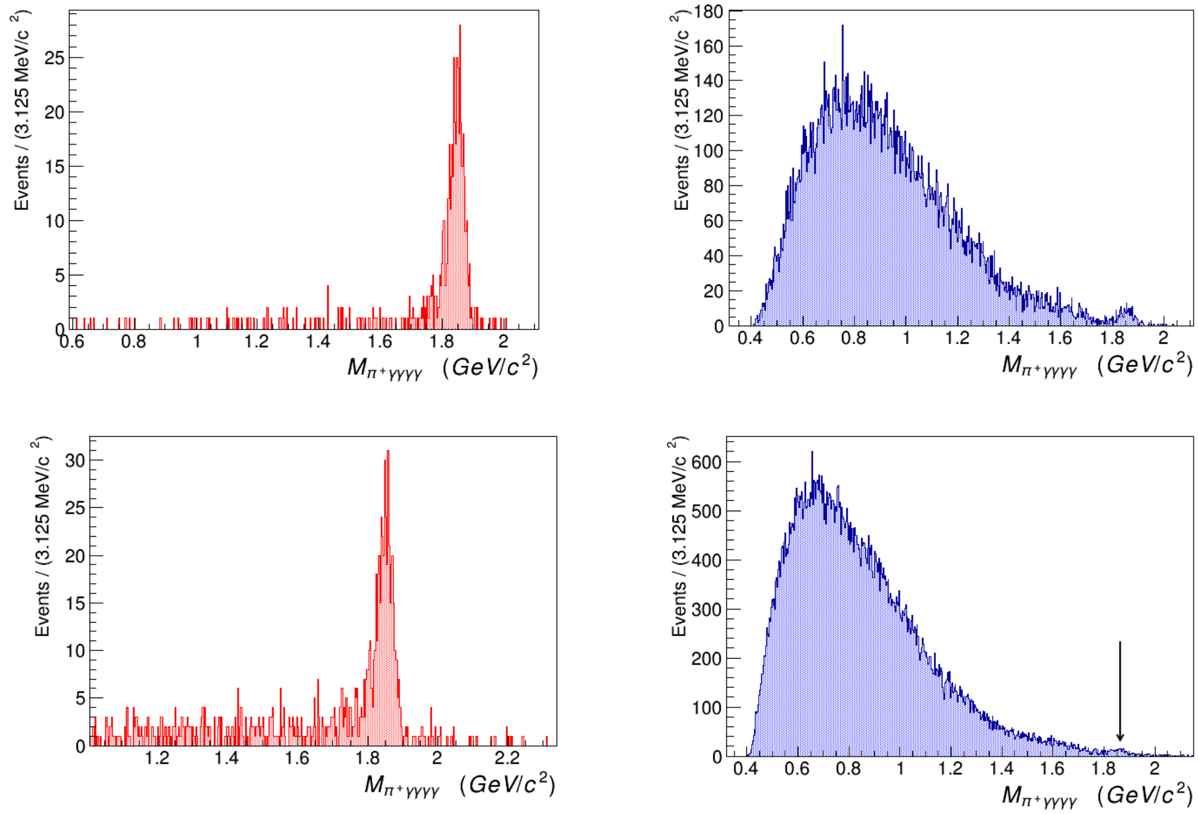

Figure 4.7: Invariant mass distribution $M_{\pi^+\gamma\gamma\gamma\gamma}$ for the exclusive MC sample (left) and the data set (right). The top row shows the results for the reconstruction of π^0 via invariant mass reconstruction with two photons. The bottom row shows the results after kinematic fitting for the reconstruction of π^0.

The detection efficiencies are calculated as explained in Section 3.3 and turn out to be $(10.0 \pm 0.3)\%$ for the first method of reconstruction for π^0 and $(11.7 \pm 0.3)\%$ when the second method is employed. Thus, it independently of the combinatorial background level, the efficiencies are almost the same. The detection efficiency for D^+ reconstruction via this channel is significantly lower than that for the reconstruction of D^- via $D^- \to K^+\pi^-\pi^-$ due to the lousy resolution of the EMC to resolve electromagnetic shower clusters. Moreover, the D^- decay involves a reconstruction with only three particles, while that for D^+ involves five particles: $\pi^+\gamma\gamma\gamma\gamma$.

The signal counts for D^+ reconstructed via its decay into $\pi^+\pi^0\pi^0$ are 128 ± 35 for the first method and 127 ± 51 for the second one (kinematic fitting for π^0 reconstruction). In the end, both methods yield the same counts despite their small difference in efficiencies. The fit results for both methods can be seen in Fig. 4.8. The signal for the first method is fitted by a Crystal Ball function, which was developed by the Crystal Ball Collaboration [36] and consists on a Gaussian with a tail on the low side commonly used to account for radiative energy loss. The signal shape for the second method is fitted by a Breit-Wigner function. The combinatorial background is modelled by a first-order Chebyshev polynomial in both cases.

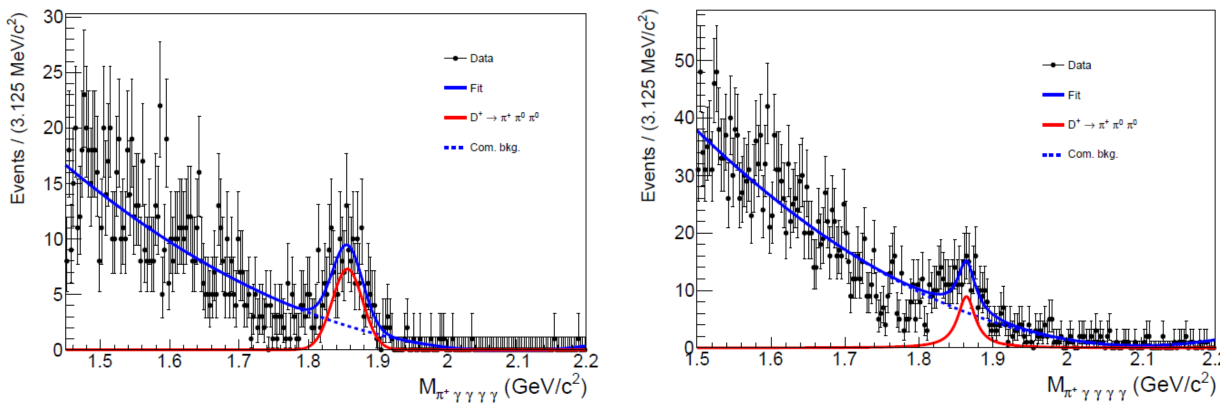

Figure 4.8: Fit results for $M_{\pi^+\gamma\gamma\gamma\gamma}$ for the first method (reconstruction of π^0 via invariant mass reconstruction with two photons, left) and the second method (kinematic fitting for the reconstruction of π^0, right). The dots represent data, the solid blue line represents the total fit, the solid red line represents the signal fit and the dashed blue line stands for the combinatorial background.

With the data available, the calculation of $\mathcal{B}(D^+ \to \pi^+\pi^0\pi^0)$ as explained in Section 3.1 gives $(9 \pm 4) \times 10^{-3}$ when π^0 invariant mass is reconstructed via photon-pair combination and $(7 \pm 4) \times 10^{-3}$ when kinematic fit is performed to build the π^0 candidates. These results are in agreement with the current PDG value, $\mathcal{B}(D^+ \to \pi^+\pi^0\pi^0) = (4.5 \pm 0.4) \times 10^{-3}$ [8], but present a higher uncertainty. The statistical error bars are larger than those for the CLEO-c results [13] for the same study due to the fact that, in this thesis, only one decay channel for the D^- decay was employed, whereas the CLEO-c study involved many more. Adding more D^- decay channels to the work in this thesis could improve up to 10 times the statistics available for the calculations.

In order to try and improve the determination of $\mathcal{B}(D^+ \to \pi^+\pi^0\pi^0)$, the difference in momentum between D^+ and D^-, $|\mathbf{p}_{D^-D^+}|$, is studied. The difference will be zero if the considered candidates for D^- and D^+ have been produced in a pair. Fig. 4.9 shows how $|\mathbf{p}_{D^-D^+}|$ exclusive MC results look when invariant mass reconstruction with two photons is performed to reconstruct π^0 (left) and when kinematic fitting is used instead (right). The exclusive MC plots are presented here because the information they portray is what allows to decide on which cuts can be done in order to improve the study.

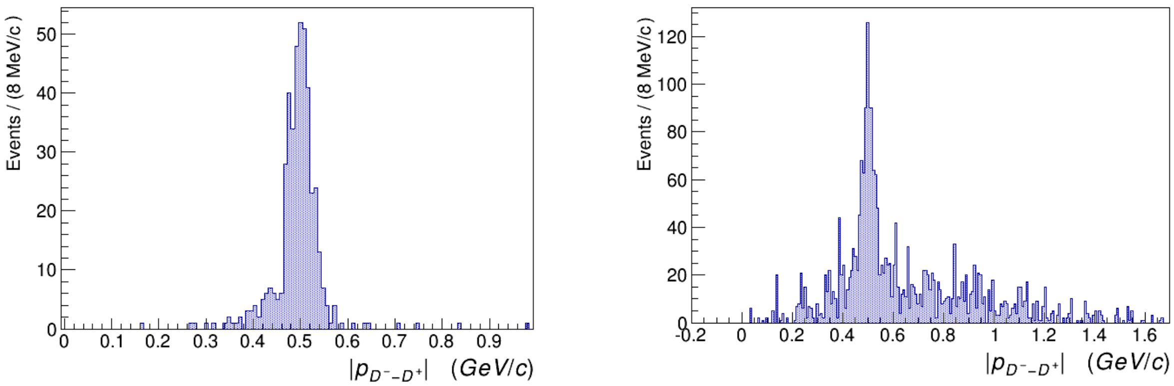

Figure 4.9: Exclusive MC results for the momentum difference between D^+ and D^- candidates, $|\mathbf{p}_{D^-D^+}|$. The left plot shows the results for the first method of π^0 reconstruction (via invariant mass reconstruction with two photons) and the right one shows the results for the second method (kinematic fitting).

In this case, the chosen cuts are $0.45 < |\mathbf{p}_{D^-D^+}|$ (GeV/c) < 0.56 for the first method of π^0 reconstruction and $0.41 < |\mathbf{p}_{D^-D^+}|$ (GeV/c) < 0.59 for the second (kinematic fitting). The results for the D^+ invariant mass spectra are shown in Fig. 4.12 with the greem line shape filled with diagonal green lines. Applying this cuts yields new D^+ signal counts and detection efficiencies: 162 ± 13 D^+ signal counts and an efficiency of $(8.4 \pm 0.3)\%$ for the first method of π^0 reconstruction; and 145 ± 94 D^+ signal counts and an efficiency of $(13.9 \pm 0.4)\%$ for the second method. The new branching fraction calculations are $\mathcal{B}(D^+ \to \pi^+\pi^0\pi^0) = 0.013 \pm 0.001$ for the first method and for the second $\mathcal{B}(D^+ \to \pi^+\pi^0\pi^0) = (7 \pm 5) \times 10^{-3}$. Even though the signal counts and efficiencies do not change dramatically after the cut, the result for the first method is not in good agreement with the current PDG value of $(4.5 \pm 0.4) \times 10^{-3}$ [8]. Thus, a study on the mass difference between ψ'' and the reconstructed D^+D^- pairs is studied.

The procedure followed in the study of the aforementioned mass difference is the same as that followed for the study of the momentum difference between the D^+D^- pair. Fig. 4.10 shows the exclusive MC results for the first method of π^0 reconstruction and the second one. Ideally, the difference should be zero. However, even though small deviations from zero are expected, it is striking how far from zero the mass difference is, and the fact that it is negative. Fig. 4.11 shows the data results for the difference in mass between ψ'' and the D^+D^- pair for when invariant mass reconstruction of π^0 is considered (left) and for when kinematic fitting is included instead (right). It is observed that the exclusive MC results are in good agreement with the data results for the first method of reconstruction for π^0, whereas for the second method the large peak when the difference is positive is not shown in exclusive MC results.

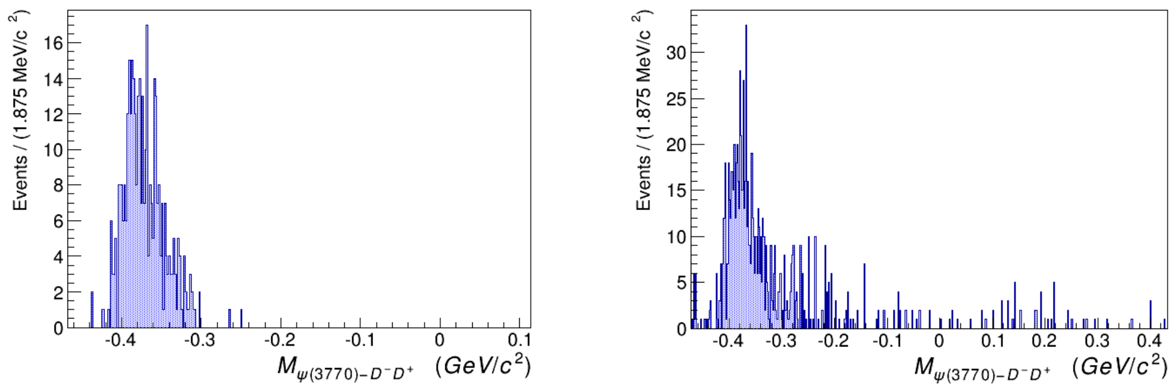

Figure 4.10: Exclusive MC results for the mass difference between $\psi(3770)$ and the D^+D^- pair candidates, $M_{\psi(3770)-D^-D^+}$. The left plot shows the results for the first method of π^0 reconstruction (via invariant mass reconstruction with two photons) and the right one shows the results for the second method (kinematic fitting).

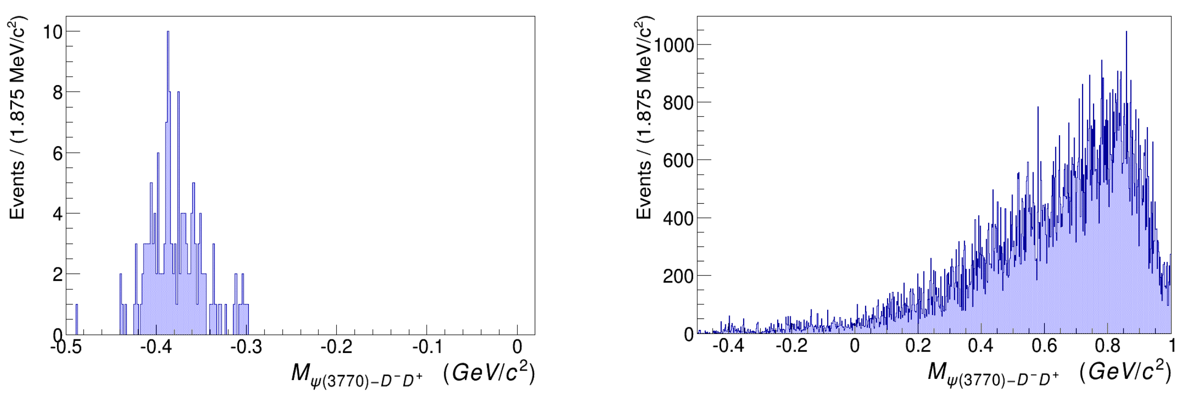

Figure 4.11: Data results for the mass difference between $\psi(3770)$ and the D^+D^- pair candidates, $M_{\psi(3770)-D^-D^+}$. The left plot shows the results for the first method of π^0 reconstruction (via invariant mass reconstruction with two photons) and the right one shows the results for the second method (kinematic fitting).

In order to make sure that there is nothing wrong with the reconstruction algorithm, the momentum of each individual D meson is checked. It is expected that $|\mathbf{p}_{D^{\pm}}|$ peaks around 0.28 GeV/c. D^- peaks at 0.25 GeV/c and D^+ also has its peak at 0.25 GeV/c for both methods of π^0 reconstruction. Thus, since this check came out right, a mass difference momentum cut is chosen: $-0.41 < M_{\psi(3770)-D^-D^+}$ $(GeV/c^2) < -0.33$ for both methods of π^0 reconstruction. This cut is based on the information provided by the exclusive MC results.

Applying the mass difference cut, together with the cut for the momentum difference, yields 130 ± 11 D^+ signal counts and an efficiency of $(7.4 \pm 0.2)\%$ for π^0 invariant mass reconstruction, which leads to a branching fraction of $(0.012 \pm 0.001$. When kinematic fitting of π^0 is employed, the D^+ curve cannot be fit. The first row of Fig. 4.12 shows how the D^+ spectrum looks before any cut is applied (blue), after the momentum constraint is applied (green diagonal lines) and after both the momentum and mass constraints are applied (red horizontal lines) for when π^0 is reconstructed via the first method (left) and the second (right). It can be observed that, for the first method, just the momentum constraint eliminates most of the combinatorial background. However, for the second method of π^0 reconstruction, that is not the case. For both methods, the momentum constraint seems to allow for slightly more events to fall under the D^+ curve for both methods. This is consistent with the number of signal counts obtained. When both the momentum and mass constraints are applied, the combinatorial background is almost completely suppressed for both π^0 reconstruction methods. Nevertheless, the curve corresponding to both constraints and kinematic fitting of π^0 (red horizontal lines, right) cannot be fit properly since some bins are too high, beyond standard fluctuations. This implies that multiple counting of π^0 is involved in the analysis and, therefore, this curve cannot be used for the analysis.

The bottom row in Fig. 4.12 shows the inclusive MC results for the reconstruction of D^+ when the first method for π^0 reconstruction is considered (left) and when the second is considered instead (right). The colours represent the same as for the plots on the first row. The inclusive MC plots show more events for $M_{\pi^+\gamma\gamma\gamma\gamma}$ than those for data because the inclusive MC sample considers more events than the data one. If the scaling factor between data and inclusive MC was known, the inclusive MC results could be scaled down to match the data. Essentially, the inclusive MC plots show very similar line shapes than those of data, but a bit more well defined. When attempting to calculate the branching fraction from inclusive MC results, the result is similar to the one obtained during the analysis. This calculation is made for the case in which the first method of reconstruction for π^0 is employed and both the momentum and mass constraints are considered. The calculation is made just for this case due to the fact that it is very simple to get the signal counts from the curve of the $\pi^+\gamma\gamma\gamma\gamma$ curve. This yields (1541130 ± 1980) signal counts for D^- and (1490 ± 39) signal counts for D^+. The efficiency for this case is $(7.4 \pm 0.2)\%$. The branching fraction calculation with these data gives (0.0133 ± 0.0005), which is in good agreement with the result obtained for data under the same conditions but different from the one used in the simulation, which was the value provided by the PDG, $(4.5 \pm 0.4) \times 10^{-3}$ [8].

The fact that the inclusive MC line shapes and results are in agreement with data results indicates that the D^+ event selection is consistent but not proper, since the value obtained for the branching fraction does not correspond to the one in the PDG, $(4.5 \pm 0.4) \times 10^{-3}$. The event selection fails to remove peaking backgrounds that are misidentified as signal events for the channel of interest. Applying cuts for momentum and mass does not help to obtain a better value of the branching fraction for any method. With the aim of trying to improve the precision of the measurements, a second analysis method is utilised. This second method is described in the following section.

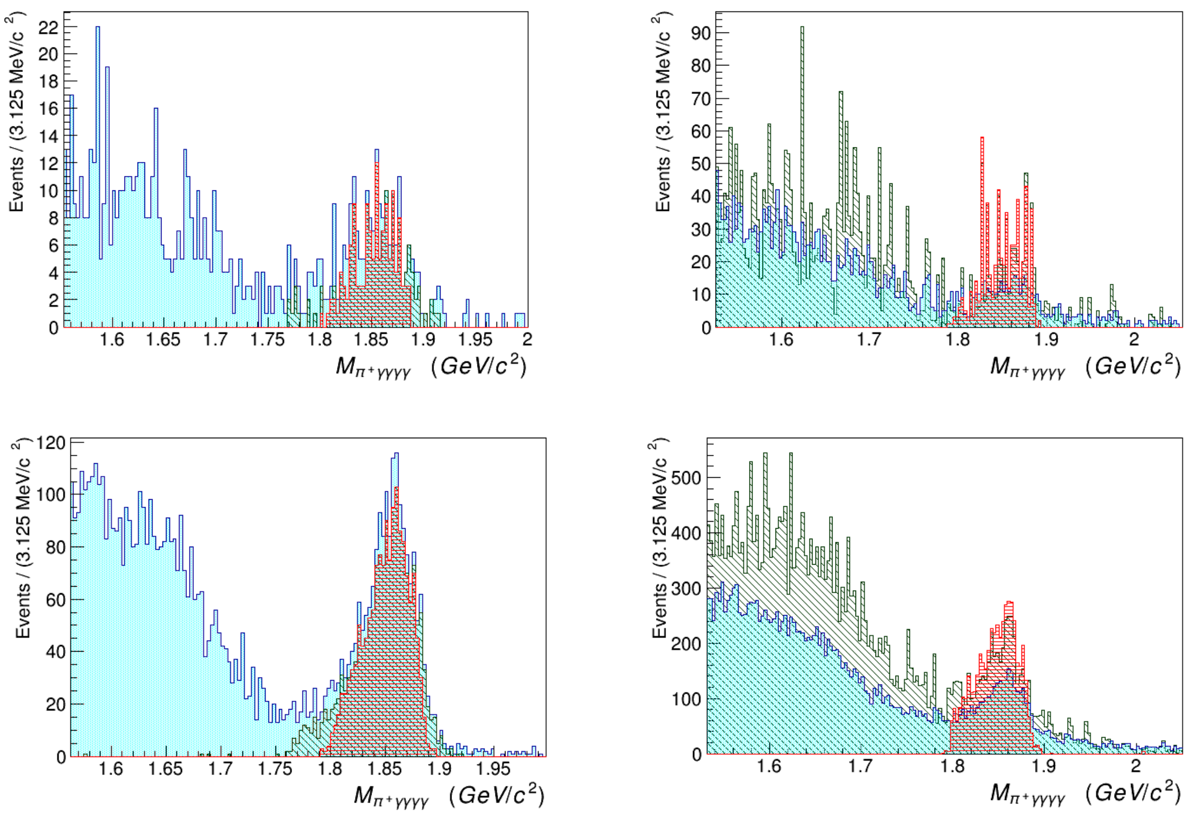

Figure 4.12: Fit results for $M_{\pi^+\gamma\gamma\gamma\gamma}$ for the first method (π^0 invariant mass reconstruction with two photons, left) and the second method (kinematic fitting for the reconstruction of π^0, right). The top row shows the results for data and the bottom row shows inclusive Monte Carlo results. The blue line represents $M_{\pi^+\gamma\gamma\gamma\gamma}$, the green line shape filled with diagonal green lines represents $M_{\pi^+\gamma\gamma\gamma\gamma}$ after the momentum cut described in the text is applied, and the red line shape filled with red horizontal lines represents $M_{\pi^+\gamma\gamma\gamma\gamma}$ after the before mentioned momentum cut plus a mass constraint, which is also explained in the text.

4.2 Reconstruction of $D^\pm$ via ΔE and M_{bc}

In this section, the reconstruction of the D mesons is done via the introduction of two kinematic variables, $\Delta E = E_{beam} - E_D$ and $M_{bc} = \sqrt{E_{beam}^2 - \mathbf{p}_D^2}$, where E_{beam} is the energy of the beam and $E_D, \mathbf{p}_D$ are the energy and momentum of the D candidate. This is the standard method for D reconstruction in experiments like BESIII or CLEO-c. In fact, it is the method followed by the CLEO-c collaboration in 2006 for the measurement of $\mathcal{B}(D^+ \to \pi^+\pi^0\pi^0)$ [13].

The utilisation of the beam-energy-constrained mass, M_{bc}, improves the mass resolution and suppresses large contributions of combinatorial background. If the D candidates are well reconstructed, ΔE shows a narrow peak around zero and M_{bc} shows a narrow peak at the D mass, $M_{D^\pm} = (1869.59 \pm 0.09)$ MeV/c^2 (PDG value [8]). In order to calculate the signal yield by fitting M_{bc}, ΔE is required to be within 3σ of the ΔE peak position.

In the following subsections, the reconstruction of D^- and D^+ (taking into account both π^0 reconstruction methods explained in 4.1.2) via these two kinematic variables is explained.

4.2.1 D^- reconstruction

The D^- candidates are reconstructed via the combination of $K^+\pi^-\pi^-$. The momentum $\mathbf{p}_D$ and energy E_D of each D^- candidate is calculated in order to build the ΔE and M_{bc} variables. The energy of the beam corresponds to half of the center-of-mass energy $\sqrt{s} = 3.773$ GeV of the data set, $E_{beam} = \sqrt{s}/2$.

ΔE for D^- is shown in Fig. 4.13. The left plot shows the exclusive MC results, while the right one shows data. For well reconstructed candidates, ΔE is expected to be centred around zero. It is observed that this is the case, even considering the amount of combinatorial background for data. The exclusive MC curve is fit by a Gaussian in order to obtain the peak position of ΔE and the standard deviation, σ. In order to build M_{bc} within $\pm 3\sigma$ of the ΔE peak, the cut applied in ΔE is $-0.01825 < \Delta E(\text{GeV}) < 0.01835$.

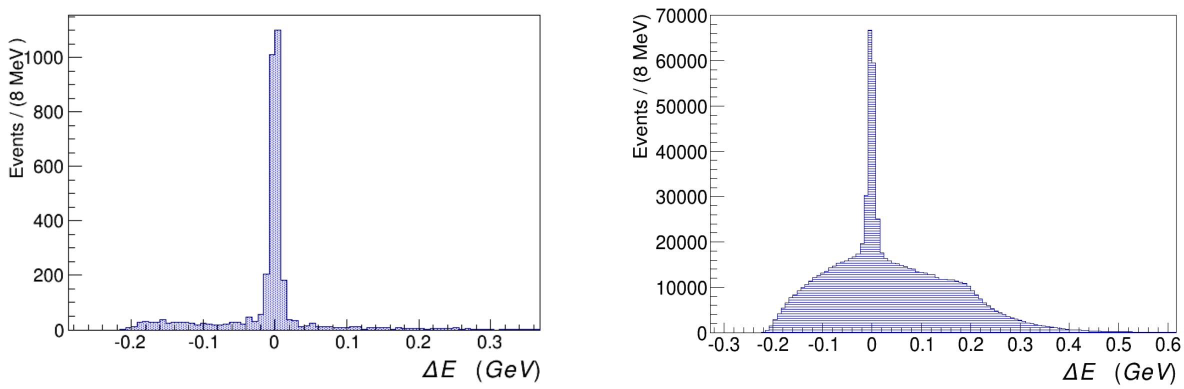

Figure 4.13: $\Delta E = E_{beam} - E_D$ for the D^- candidates. The left plot shows exclusive MC results, while the right one shows data.

The fit results for the beam-energy-constrained mass, M_{bc}, of D^- are shown in Fig. 4.14. The signal curve is fit by a Crystal Ball function and the background is modelled with a first-order Chebyshev polynomial function. It is evident that this D^- reconstruction method provides a much cleaner spectrum in regards of combinatorial background than the invariant mass reconstruction from its decay products. The signal yield is 116179 ± 439.

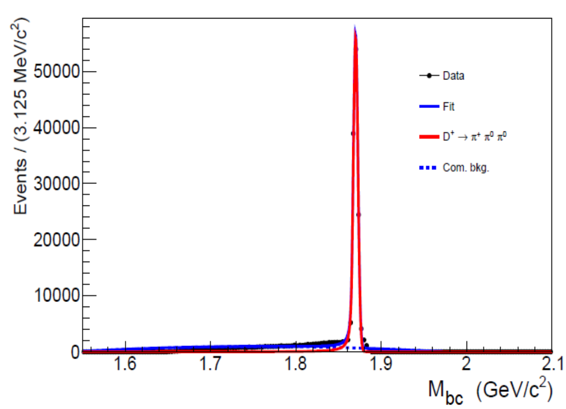

Figure 4.14: Fit results for the beam-energy-constrained mass, $M_{bc} = \sqrt{E_{beam}^2 - \mathbf{p}_D^2}$, for the D^- candidates. The solid blue line represents the total fit, the solid red line represents the signal fit and the dashed blue line represents the combinatorial background.

4.2.2 D^+ reconstruction

For the decay of interest, $D^+ \to \pi^+\pi^0\pi^0$, the D^+ candidates are reconstructed taking into account two different methods for π^0 reconstruction: π^0 invariant mass reconstruction via combination of photon pairs (first method) and kinematic fitting of π^0 (second method). The details for each π^0 reconstruction method are given in Section 4.1.2. This leads to two different D^+ reconstruction results: one for the first method of π^0 reconstruction and another one for the second method.

As explained in Section 4.1.3, a cut on the goodness-of-fit χ^2_{KF} for the kinematic fit of π^0 is performed in order to improve the signal-to-background ratio. Fig. 4.15 shows the dependence of the significance $N_{sig}/\sqrt{N_{sig} + N_{bkg}}$ on the value of the χ^2_{KF}, where N_{sig} is the number of signal counts and N_{bkg} is the number of background counts. The cut is chosen to be $\chi^2_{KF} < 75$. This value was chosen due to the fact that it is located in the saturation region for the significance.

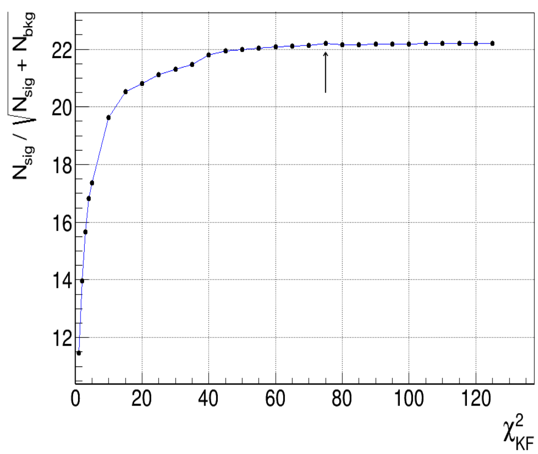

Figure 4.15: Statistical significance $N_{sig}/\sqrt{N_{sig} + N_{bkg}}$ versus different χ^2_{KF} values, where KF stands for kinematic fitting. A cut on $\chi^2_{KF} < 75$ was chosen, indicated with an arrow on the plot.

Following the same procedure as for the D^- reconstruction, ΔE is calculated for both the D^+ candidates reconstructed by taking into consideration the first method of π^0 reconstruction and those built by involving the second method instead. Fig. 4.16 shows the exclusive MC and data curves for the first method and 4.17 shows the same when kinematic fitting of π^0 is considered.

In Fig. 4.16, when π^0 invariant mass is reconstructed, the implemented ΔE constraint is $-0.097 < \Delta E$ (GeV) < 0.047. It is observed that, in this case, a very small peak around zero appears for data and, instead, a large, wide peak makes an appearance at around -0.9 GeV. This can be explained by the contribution of unrelated tracks that were misidentified and included in the D^+ candidate reconstruction. Since they were not identified correctly, the D^+ energy is not around the beam energy and ΔE is not zero.

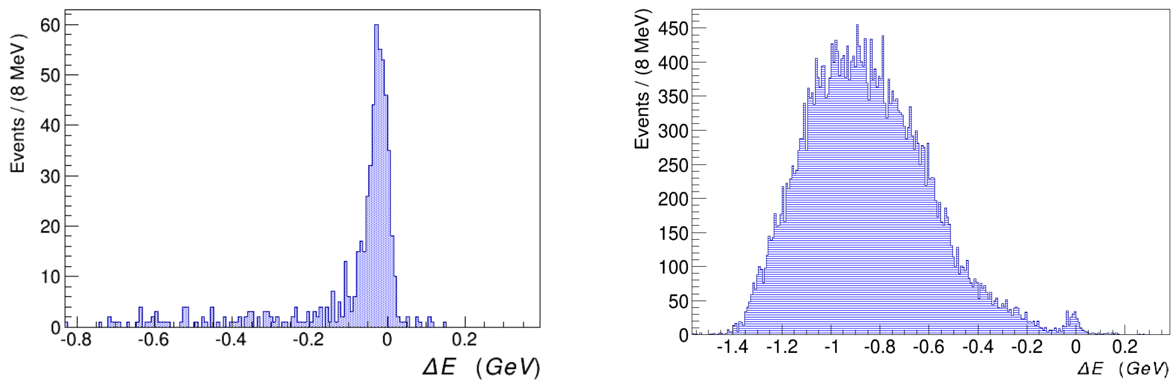

Figure 4.16: $\Delta E = E_{beam} - E_D$ for the D^+ candidates when π^0 invariant mass reconstruction is considered. The left plot shows exclusive MC results, while the right one shows data.

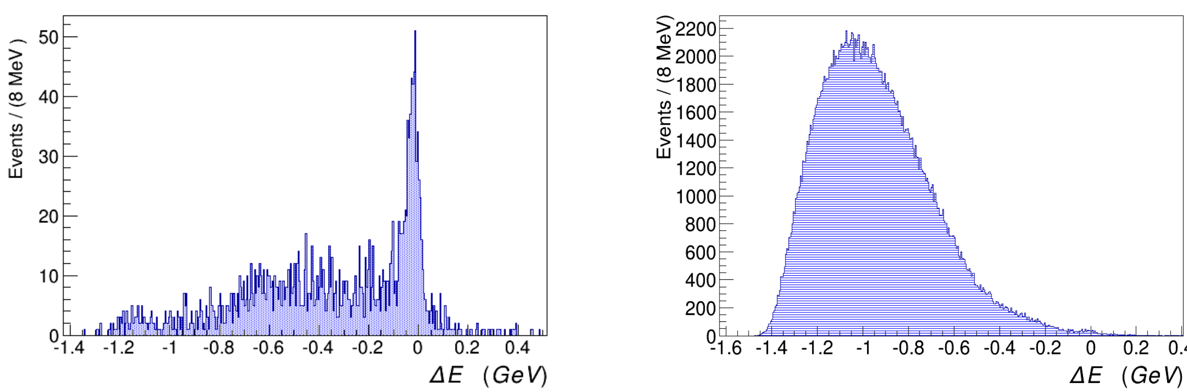

Figure 4.17: $\Delta E = E_{beam} - E_D$ for the D^+ candidates when kinematic fitting is considered for the π^0 reconstruction. The left plot shows exclusive MC results, while the right one shows data.

Fig. 4.17 shows the ΔE curves for exclusive MC and data when kinematic fitting is used for the reconstruction of π^0. For this method, the ΔE constraint is $-0.096 < \Delta E$ (GeV) < 0.048. The expected peak around zero is almost non-existent in data, and the number of events included in the wide peak appearing around -1 GeV is much larger than that for the π^0 reconstruction method. These results back the hypothesis that many tracks that are not of relevance for this process have been included in the analysis, making the results for the D^+ reconstruction via kinematic fitting of π^0 unreliable.

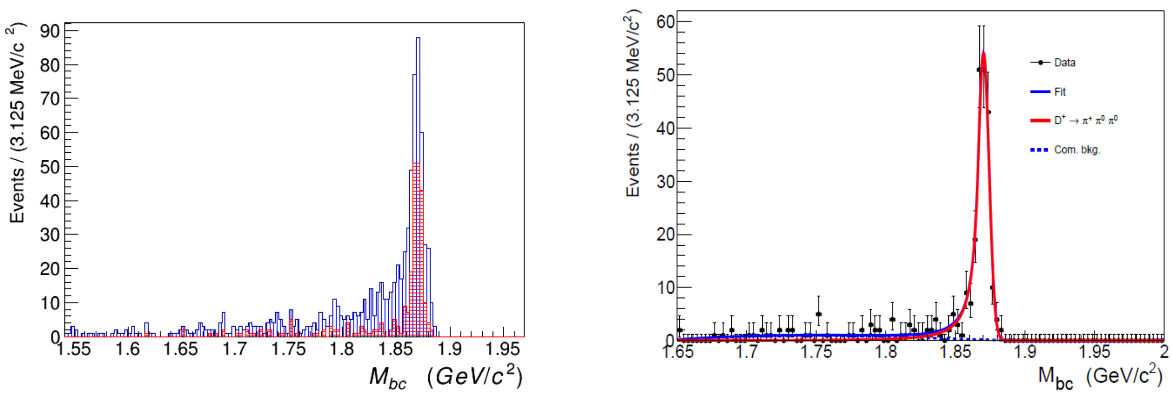

Figure 4.18: Beam-energy-constrained mass M_{bc} of the D^+ candidates. The left plot shows the M_{bc} results for the π^0 invariant mass reconstruction (red horizontal lines) and for when kinematic fitting is employed instead (blue vertical lines). The right plot shows the fit results for the first method of π^0 reconstruction (π^0 invariant mass reconstruction with two photons). The dots represent data, the solid blue line represents the total fit, the solid red line represents the signal fit and the dashed blue line stands for the combinatorial background.

The beam-energy-constrained mass M_{bc} is shown in Fig. 4.18 for both π^0 reconstruction methods. Drawn in blue vertical lines is the result for when kinematic fitting is employed for the π^0 reconstruction, whereas the curve filled with red horizontal lines represents the result after π^0 invariant mass reconstruction. It is observed that when kinematic fitting is considered, the curve presents a tail on the left side that unavoidably includes background counts to the signal region. From this observed curve shape, together with the information obtained from the ΔE analysis, it is concluded that the D^+ reconstruction method in which π^0 kinematic fitting is considered is not valid for this analysis. However, the curve for when a π^0 invariant mass reconstruction is performed appears to be appropriate for further analysis. Therefore, that curve is fit in order to obtain the signal yield. The fit is shown on the right plot of Fig. 4.18. The signal shape is fit by a Crystal Ball function and the background is fit by a second-order Chebyshev polynomial function. The signal yield is 286 ± 16 events and the D^+ candidates are reconstructed with an efficiency of $(9.666 \pm 0.006)\%$. With these data, the branching fraction is calculated to be $\mathcal{B}(D^+ \to \pi^+\pi^0\pi^0) = 0.020 \pm 0.001$, which is about 1.5 times higher than all of the results obtained in Section 4.1. In addition, this obtained value is about four times higher than the value published by the PDG, $(4.5 \pm 0.4) \times 10^{-3}$ [8].

The branching fraction can also be calculated from inclusive MC results. The signal yield for D^- for the inclusive MC sample is 1350380 ± 1162, while that for the D^+ candidates reconstructed via π^0 invariant mass reconstruction is 2030 ± 45. This corresponds to a branching fraction of 0.0159 ± 0.0003, which is about 1.25 times lower than the value obtained with data. The fact that this method fails to resolve the branching fraction suggests that there may be some other interfering channels in this reconstruction that do not allow a proper measurement of the correct number of D^+.

4.3 Results and discussion

The branching fraction $\mathcal{B}(D^+ \to \pi^+\pi^0\pi^0)$ calculation is done by means of equation 3.1:

$$\mathcal{B}(D^+ \to \pi^+\pi^0\pi^0) = \frac{N_{sig}^{D^+}}{N_{sig}^{D^-} \cdot \epsilon_{D^+} \cdot \mathcal{B}(\pi^0 \to \gamma\gamma) \cdot \mathcal{B}(\pi^0 \to \gamma\gamma)}$$

where $N_{sig}^{D^+}$ is the number of signal events for D^+, $N_{sig}^{D^-}$ is the number of signal events for D^-, ϵ_{D^+} is the D^+ detection efficiency and $\mathcal{B}(\pi^0 \to \gamma\gamma)$ is the branching ratio for the decay of π^0 into a photon pair. The results for the branching fraction calculation of $D^+ \to \pi^+\pi^0\pi^0$ for each of the methods explained throughout this chapter are summarised in Table 4.1.

Invariant mass reconstruction of D mesons seems to yield better results than the reconstruction via ΔE and M_{bc}, and the results from both methods are not consistent between them. The best result was obtained for the invariant mass reconstruction of the D mesons by applying the momentum constraint and kinematic fitting for π^0. The number of reconstructed D^+ seems to be consistent for each of the different methods applied when invariant mass reconstruction of D^+ is performed. However, the signal counts for D^+ when ΔE and M_{bc} are employed for the reconstruction of D^+ are about 1.5 times higher than those from invariant mass reconstruction of D^+. This may have an explanation of other interfering decay channels of D^+ that do not allow for a proper reconstruction from the channel of interest.

The reconstruction of D mesons via the two kinematic variables ΔE and M_{bc} is the standard method utilised by the BESIII and CLEO-c collaborations. In the 2006 analysis made by CLEO-c for the measurement of $\mathcal{B}(D^+ \to \pi^+\pi^0\pi^0)$ [13], this is the method utilised. In that publication, the π^0 are formed from photon pairs that have an invariant mass within 3σ of the π^0 mass. Then, a kinematic fit that constrains the mass of the two photons to the π^0 mass is performed. This method is described in [37]. For the D reconstruction from decay channels with three or more pions, they applied a veto on any candidate containing a π^0 pair: $475 < M_{\pi^0\pi^0}$ (MeV/c^2) < 548. This cut is made in order to suppress a large background generated by K_S^0 decays. Applying this cut on the work in this thesis could refine the counting of D^+ signal events of interest. Since the reconstruction of D mesons via ΔE and M_{bc} allows for a cleaner spectrum of the D invariant mass, this method is the recommended one to continue the analysis on. Other contributions to this channel, like $K_S^0 \to \pi^0\pi^0$ should be substracted in order to purify the event selection.

	D^+ inv. mass reconst.						D^+ reconst. via ΔE, M_{bc}	
	No cuts in D^+		$\overrightarrow{p}$ **cut**		$\overrightarrow{p}$ **and M cuts**		π^0 **A**	π^0 **B**
	π^0 **A**	π^0 **B**	π^0 **A**	π^0 **B**	π^0 **A**	π^0 **B**		
$N_{sig}^{D^-}$	150071 ± 1194						116179 ± 439	
$N_{sig}^{D^+}$	128 ± 35	127 ± 51	163 ± 13	145 ± 94	130 ± 11	-	218 ± 16	-
ϵ_{D^+} (%)	10.0 ± 0.3	11.7 ± 0.3	8.4 ± 0.3	13.9 ± 0.4	7.4 ± 0.2	-	9.666 ± 0.006	12.004 ± 0.006
$\mathcal{B}$ (10^{-3})	9 ± 4	7 ± 4	13 ± 1	7 ± 5	12 ± 1	-	20 ± 1	-
PDG [8] $\mathcal{B}$ (10^{-3})	4.5 ± 0.4							

Table 4.1: Summary of the results $\mathcal{B}(D^+ \to \pi^+\pi^0\pi^0)$ for the analysis of 2010 data from BESIII. π^0 **A** refers to the reconstruction of D^+ when π^0 invariant mass reconstruction is considered. π^0 **B** refers to the reconstruction of D^+ when π^0 kinematic fitting is considered.

Chapter 5

Analysis of $D^+ \to \pi^+\pi^0\pi^0$ with 2011 data from BESIII at $\sqrt{s} = 3.773$ GeV

The analysis in this chapter is made on data collected by BESIII at the ψ'' resonance energy, $\sqrt{s} = 3.773$ GeV. The data collection took place from December 2010 to May 2011 with an integrated luminosity of $(1989.27 \pm 0.15 \pm 19.89)$ pb^{-1} [14], where the first error is statistical and the second systematic. The total number of D^+D^- events is calculated to be $(56.30 \pm 0.22) \cdot 10^5$, and is estimated following the same procedure explained in the beginning of Chapter 4.

The analysis procedure is the same employed in the previous chapter for the 2010 data. Results for both data and Monte Carlo simulations will be discussed. Two different approaches are considered for the reconstruction of the $D^\pm$ candidates, resembling those discussed in Chapter 4: one based in invariant mass reconstruction of the D mesons via their decay products (results discussed in Section 5.1), and another one based on the usage of the two kinematic variables, $\Delta E = E_{beam} - E_D$ and $M_{bc} = \sqrt{E^2_{beam} - \mathbf{p}^2_D}$, where E_{beam} is the beam energy and E_D, $\mathbf{p}^2_D$ are the energy and momentum of the D candidate (results discussed in Section 5.2.

All of the results and cuts made from exclusive MC results in Chapter 4 apply to the analysis described in this chapter. The data reconstruction and generation of the MC samples was done with the BESIII Offine Software System (BOSS) (version 6.6.4), described in 2.2.1. The ROOT [29] software, including the ROOFIT library, was employed for the data analysis.

The event selection for the process $D^+ \to \pi^+\pi^0\pi^0$ is described in Sections 3.1 and 3.2. The D^+ candidates are reconstructed by considering that they were produced in pairs with D^- mesons, which are reconstructed via the $D^- \to K^+\pi^-\pi^-$ decay channel. Therefore, events with at least one K^+ and two π^- are stored for further analysis.

5.1 Invariant mass reconstruction of $D^{\pm}$

5.1.1 D^{-} reconstruction

Kaons and pions suitable for the reconstruction of D^{-} are identified with the information from different subdetectors, like the MDC or the TOF. The invariant mass distribution of $K^{+}\pi^{-}\pi^{-}$, $M_{K^{+}\pi^{-}\pi^{-}}$, is calculated and plotted in order to reconstruct D^{-}. This is shown for both exclusive MC and data in Fig. 5.1.

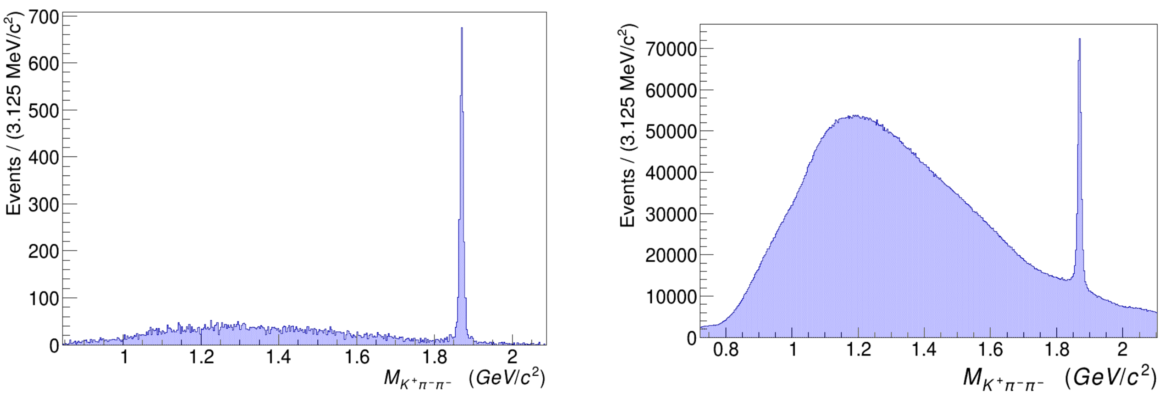

Figure 5.1: Invariant mass distribution $M_{K^{+}\pi^{-}\pi^{-}}$ for the exclusive MC sample (left) and the data set (right).

It can be seen that there is a large combinatorial background for data, but the D^{-} resonance appears very clearly at approximately its mass, $M_{D^{\pm}} = (1869.59 \pm 0.09)$ MeV/c^2 (PDG value [8]). Moreover, the line shape is very similar to that for 2010 data, the only difference being the amount of events, which has its explanation on a data set with a larger integrated luminosity than that of 2010.

The fitting results of the resonance peak are shown in Fig. 5.2. The signal line shape is taken as a Breit-Wigner function and the combinatorial background is fitted via a second-order Chebyshev polynomial function. The total fit is of the signal and background is given by a probability density function (PDF) described by the sum of the signal line shape and the background. The signal yield obtained after the fit is of 329868 ± 1750 $D^{-} \to K^{+}\pi^{-}\pi^{-}$ events.

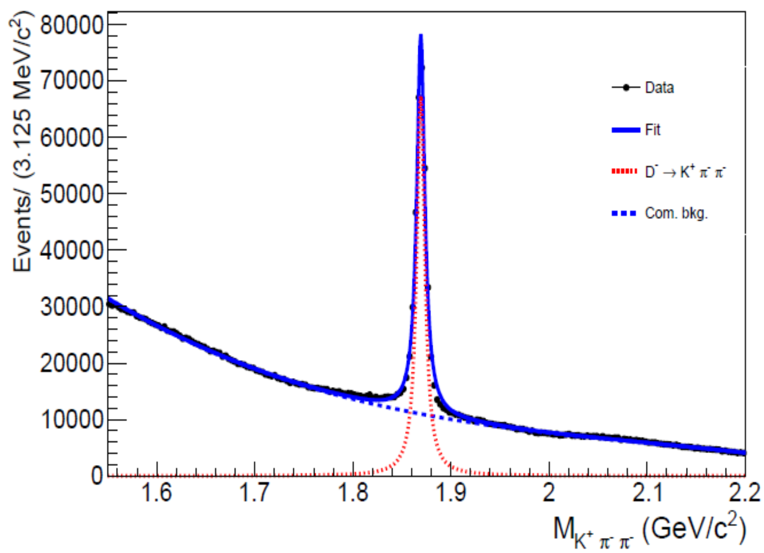

Figure 5.2: Fit result for the invariant mass distribution $M_{K^+\pi^-\pi^-}$ that corresponds to the channel $D^- \to K^+\pi^-\pi^-$. The dots represent data, the solid (blue) line represents the total fit, the dotted red line represents the signal fit and the dashed blue line represents the combinatorial background.

5.1.2 D^+ reconstruction

The D^+ candidates are reconstructed from the Cabibbo-suppressed decay of interest for this work, $D^+ \to \pi^+\pi^0\pi^0$. The pion is identified via the prodecure described in Section 3.2, whereas the π^0 candidates are reconstructed from a pair of photons in the two ways described in Section 4.1.2: via π^0 invariant mass reconstruction (first method for π^0 reconstruction from here on) and via kinematic fitting (second method for π^0 reconstruction from here on). The results for the D^+ reconstruction considering both methods for π^0 identification are shown in this section.

The invariant mass distribution $M_{\pi^+\gamma\gamma\gamma\gamma}$ is shown in Fig. 5.3. The first row shows the results for exclusive MC and data for the case in which the first method for π^0 reconstruction is used. In the second row, the results for exclusive MC and data for the second method are shown. The combinatorial background in data is much larger when kinematic fitting is used than when it is not, and also the signal peak for D^+ is much dimmer in that case.

The detection efficiencies are calculated from the exclusive MC results as explained in Section 3.3 and are $(10.0 \pm 0.3)\%$ for the first method of reconstruction for π^0 and $(11.7 \pm 0.3)\%$ when the second method is utilised. The efficiencies are very similar regardless of the method, and their low values have an explanation on the lousy resolution of the EMC to resolve electromagnetic shower clusters.

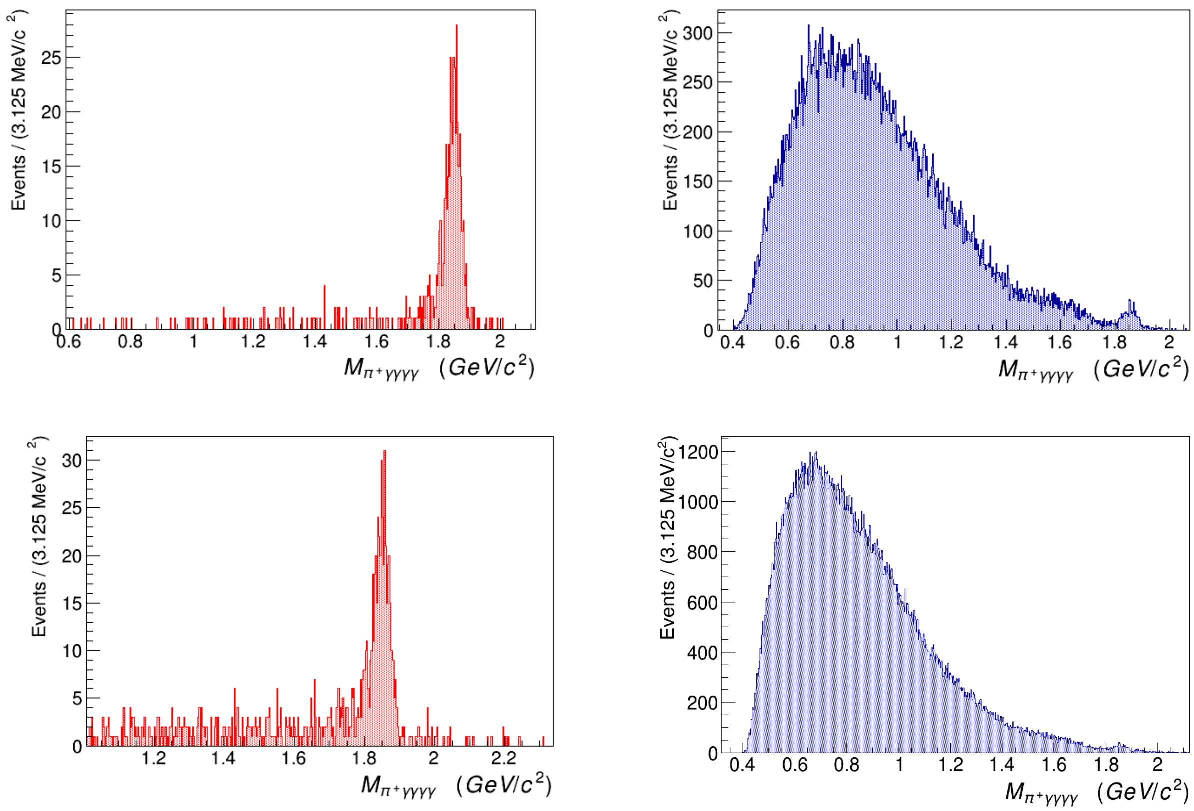

Figure 5.3: Invariant mass distribution $M_{\pi^+\gamma\gamma\gamma\gamma}$ for the exclusive MC sample (left) and the data set (right). The top row shows the results for the reconstruction of π^0 via invariant mass reconstruction with two photons. The bottom row shows the results after kinematic fitting for the reconstruction of π^0.

The fit results for the D^+ peak produced by using both π^0 reconstruction methods are shown in Fig. 4.8. The signal shape for the first method is fit by a Crystal Ball function and the background is fit by a second-order Chebyshev polynomial. The signal shape for the second method is fit by a Breit-Wigner function and the combinatorial background is modelled by a first-order Chebyshev polynomial. The signal counts for D^+ reconstructed via the first π^0 reconstruction method are 329 ± 54 and for the second method 454 ± 75.

The calculation of $\mathcal{B}(D^+ \to \pi^+\pi^0\pi^0)$ as explained in Section 3.1 gives (0.010 ± 0.002) when π^0 invariant mass is reconstructed via photon-pair combination and (0.012 ± 0.002) when kinematic fit is performed to build the π^0 candidates. These results are not in good agreement with the current PDG value, $\mathcal{B}(D^+ \to \pi^+\pi^0\pi^0) = (4.5 \pm 0.4) \times 10^{-3}$ [8].

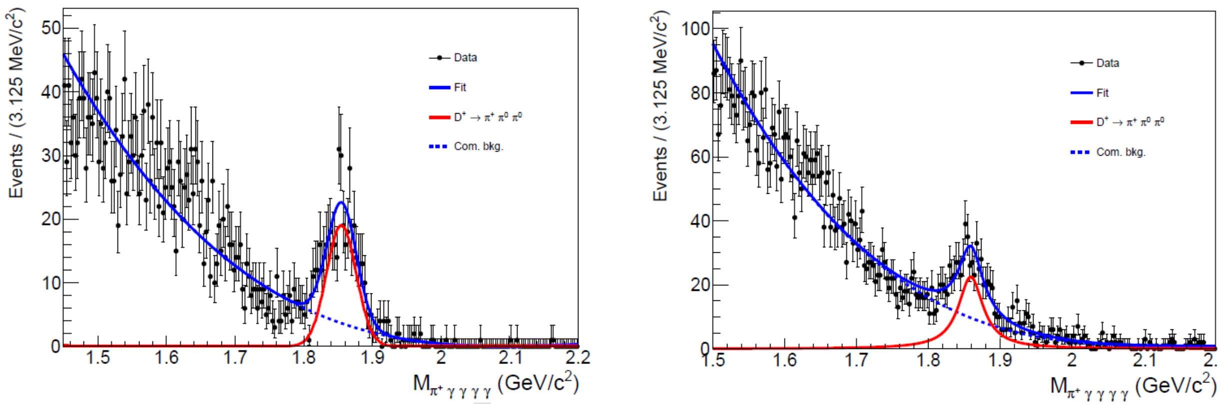

Figure 5.4: Fit results for $M_{\pi^+\gamma\gamma\gamma\gamma}$ for the first method (reconstruction of π^0 via invariant mass reconstruction with two photons, left) and the second method (kinematic fitting for the reconstruction of π^0, right). The dots represent data, the solid blue line represents the total fit, the solid red line represents the signal fit and the dashed blue line stands for the combinatorial background.

In order to try and improve the determination of $\mathcal{B}(D^+ \to \pi^+\pi^0\pi^0)$, the difference in momentum between D^+ and D^-, $|\mathbf{p}_{D^-D^+}|$, is studied. The difference will be zero if the considered candidates for D^- and D^+ have been produced in a pair. Two constraints for this momentum difference, one for each of the π^0 reconstruction methods, are chosen from exclusive MC results: $0.45 < |\mathbf{p}_{D^-D^+}|$ $(GeV/c) < 0.56$ for the first method and $0.41 < |\mathbf{p}_{D^-D^+}|$ $(GeV/c) < 0.59$ for the second (kinematic fitting). The motivation for this cuts can be found in Section 4.2.2. Applying this cut yields new D^+ signal counts and detection efficiencies for the first method of π^0 reconstruction: 341 ± 18 D^+ counts and an efficiency of $(8.4 \pm 0.3)\%$, which yields a branching fraction of (0.0126 ± 0.0008). For the second method, kinematic fitting, there is no recognisable peak that can be fit and, therefore, the signal yield cannot be obtained. Thus, the result obtained for the first method is not in good agreement with the current PDG value and a result cannot be drawn from the second method. Thus, a study on the mass difference between ψ'' and the reconstructed D^+D^- pairs is studied.

When performing a second cut on the mass difference between ψ'' and the reconstructed D^+D^- pairs as explained in Section 4.2.2, the signal yield is 272 ± 16 D^+ signal counts and an efficiency of $(7.4 \pm 0.2)\%$ for π^0 invariant mass reconstruction, which leads to a branching fraction of $(0.0114 \pm 0.0007$. When kinematic fitting of π^0 is employed instead, the D^+ curve cannot be fit, just like it occurred for the 2010 data set. The first row of Fig. 5.5 shows how the D^+ spectrum looks before any cut is applied (blue), after the momentum constraint is applied (green diagonal lines) and after both the momentum and mass constraints are applied (red horizontal lines) for when π^0 is reconstructed via the first method (left) and the second (right). It can be observed that, for the first method, just the momentum constraint eliminates most of the combinatorial background. However, for the second method of π^0 reconstruction, that is not the case. When both the momentum and mass constraints are applied, the combinatorial background is almost completely suppressed for both π^0 reconstruction methods. Nevertheless, when kinematic fitting of π^0 is considered, the curves corresponding to when the momentum constraint is applied and to when both the momentum and mass constraints are applied (green diagonal lines and red horizontal lines, right) cannot be fit properly.

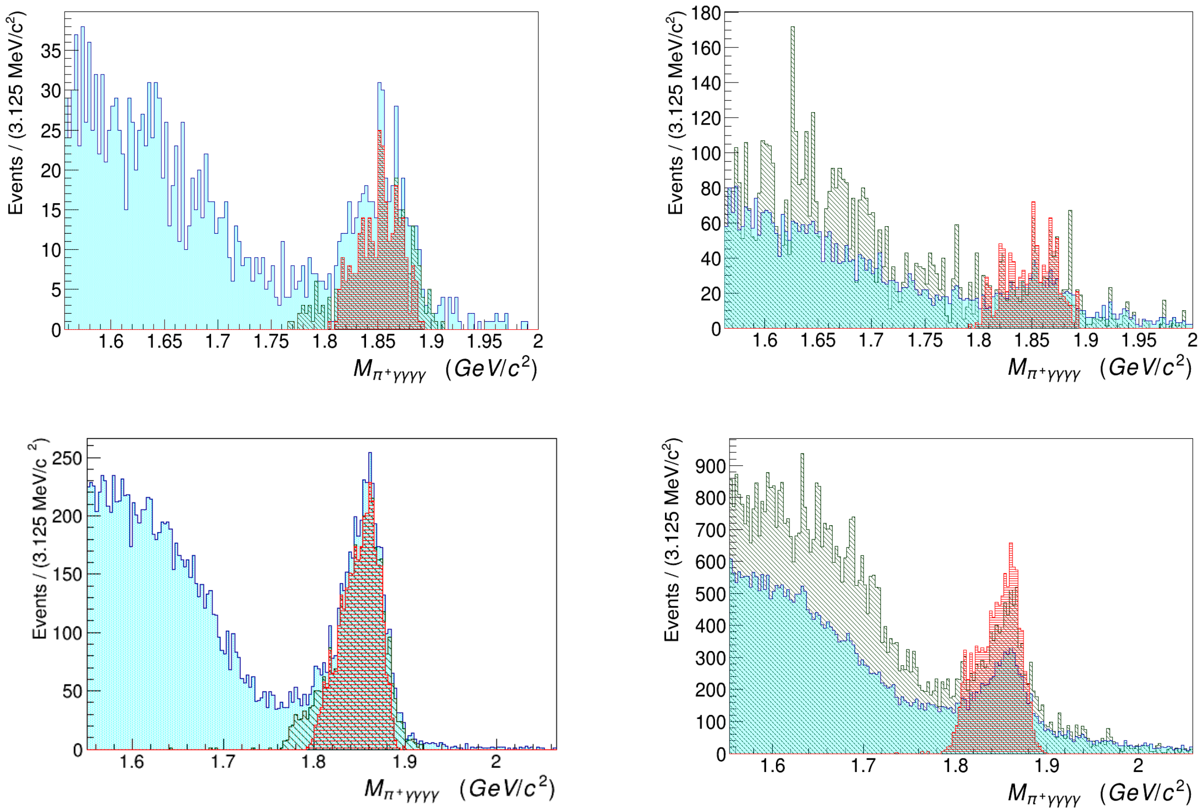

Figure 5.5: Fit results for $M_{\pi^+\gamma\gamma\gamma\gamma}$ for the first method (π^0 invariant mass reconstruction with two photons, left) and the second method (kinematic fitting for the reconstruction of π^0, right). The top row shows the results for data and the bottom row shows inclusive Monte Carlo results. The blue line represents $M_{\pi^+\gamma\gamma\gamma\gamma}$, the green line shape filled with diagonal green lines represents $M_{\pi^+\gamma\gamma\gamma\gamma}$ after the momentum cut described in the text is applied, and the red line shape filled with red horizontal lines represents $M_{\pi^+\gamma\gamma\gamma\gamma}$ after the before mentioned momentum cut plus a mass constraint, which is also explained in the text.

The bottom row in Fig. 5.5 shows the inclusive MC results for the reconstruction of D^+ when the first method for π^0 reconstruction is considered (left) and when the second is considered instead (right). The colours represent the same as for the plots on the first row. The inclusive MC plots show more events for $M_{\pi^+\gamma\gamma\gamma\gamma}$ than those for data because the inclusive MC sample contains more events than the data one. If the scaling factor between data and inclusive MC was known, the inclusive MC results could be scaled down to match the data. The inclusive MC plots show very similar line shapes than those of data, but a bit more well defined. This is very clear for the case in which kinematic fitting is employed. The branching fraction can be calculated for inclusive MC results in order to compare it with data. In this case, the value is only calculated for the case in which the first π^0 reconstruction method is utilised and both the momentum and mass constraints are in place. This choice is based on the fact that that curve presents the least difficulties to be fit. The signal count for D^- is (3369270 ± 2926), the signal yield for D^+ is (3333 ± 58) and the efficiency in this case is $(7.4 \pm 0.2)\%$. This yields a branching fraction of (0.0136 ± 0.0004), which is a similar result to the one obtained for data analysis under the same conditions.

The fact that the inclusive MC line shapes and results are in agreement with data results suggests that the D^+ event selection is consistent but not proper, since the value obtained for the branching fraction does not correspond to the one in the PDG, $(4.5 \pm 0.4) \times 10^{-3}$. The event selection fails to remove peaking backgrounds that are misidentified as signal events for the channel of interest. Applying cuts for momentum and mass does not help to obtain a better value of the branching fraction for any method. With the aim of trying to improve the precision of the measurements, a second analysis method is utilised. This second method is described in the following section.

5.2 Reconstruction of $D^\pm$ via ΔE and M_{bc}

In this section, the reconstruction of the D mesons is done via the introduction of two kinematic variables, $\Delta E = E_{beam} - E_D$ and $M_{bc} = \sqrt{E^2_{beam} - \mathbf{p}^2_D}$, where E_{beam} is the energy of the beam and $E_D, \mathbf{p}_D$ are the energy and momentum of the D candidate. This is the standard method for D reconstruction in experiments like BESIII or CLEO-c.

If the D candidates are well reconstructed, ΔE shows a narrow peak around zero and M_{bc} shows a narrow peak at the D mass, $M_{D^\pm} = (1869.59 \pm 0.09)$ MeV/c^2 (PDG value [8]). In order to calculate the signal yield by fitting M_{bc}, ΔE is required to be within 3σ of the ΔE peak position.

In the following subsections, the reconstruction of D^- and D^+ (taking into account both π^0 reconstruction methods explained in 4.1.2) via these two kinematic variables is explained.

5.2.1 D^- reconstruction

The D^- candidates are reconstructed via the combination of $K^+\pi^-\pi^-$. The momentum $\mathbf{p}_D$ and energy E_D of each D^- candidate is calculated in order to build the ΔE and M_{bc} variables. The energy of the beam corresponds to half of the center-of-mass energy $\sqrt{s} = 3.773$ GeV of the data set, $E_{beam} = \sqrt{s}/2 = 1886.5$ GeV.

ΔE for D^- is shown in Fig. 5.6. Exclusive MC results are shown on the left, while the data results are shown in the right. It can be observed that ΔE is indeed centered in zero, despite of the combinatorial background for data. The cut on ΔE is taken from the exclusive MC results, and it is $-0.01825 < \Delta E(\text{GeV}) < 0.01835$ for ΔE to be within $\pm 3\sigma$ of the ΔE peak position.

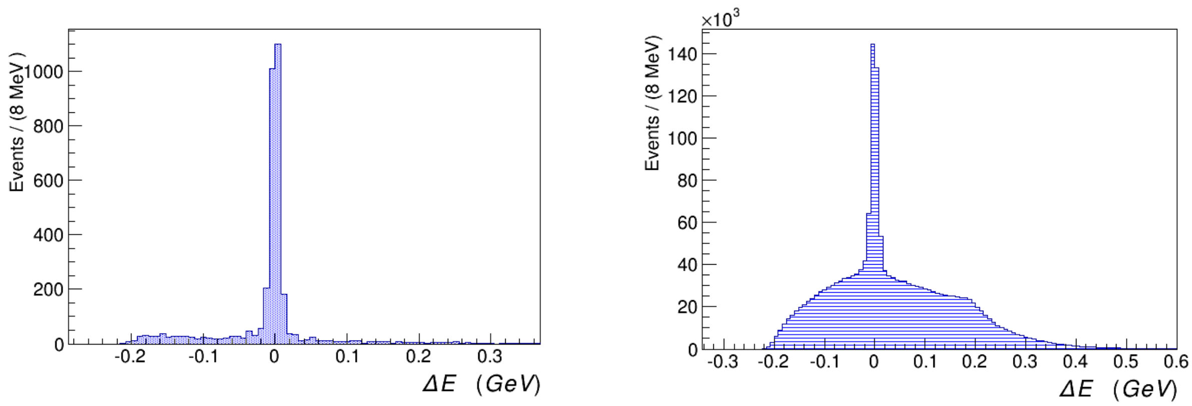

Figure 5.6: $\Delta E = E_{beam} - E_D$ for the D^- candidates. The left plot shows exclusive MC results, while the right one shows data.

The fit results for the beam-energy-constrained mass, M_{bc}, of D^- are shown in Fig. 5.7. The signal curve is fit by a Crystal Ball function and the background is modelled with a first-order Chebyshev polynomial function. It can be seen very clearly that this reconstruction method provides a much cleaner spectrum in regards of combinatorial background than the one employed in Section 5.1. The signal yield is 254967 ± 646.

5.2.2 D^+ reconstruction

The D^+ candidates are reconstructed from the decay products of the decay of interest, $\pi^+\pi^0\pi^0$, taking into account two different methods for π^0 reconstruction: π^0 invariant mass reconstruction via combination of photon pairs (first method) and kinematic fitting of π^0 (second method). The details for each π^0 reconstruction method are given in Section 4.1.2.

As it was done for the D^- reconstruction, ΔE is calculated for both the D^+ candidates reconstructed by taking into consideration the first method of π^0 reconstruction and those built with the second method instead. Fig. 5.8 shows the exclusive MC and data curves for the first method and 5.9 shows the same when kinematic fitting of π^0 is considered.

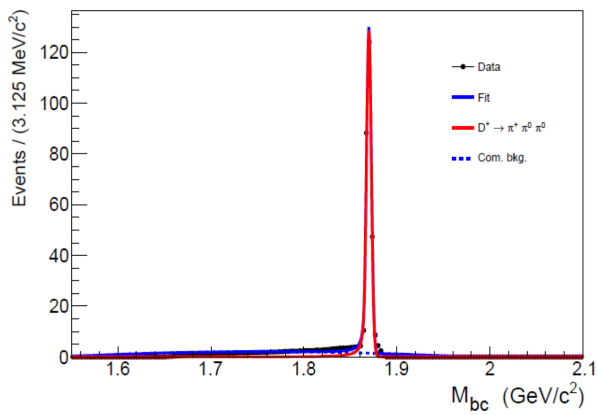

Figure 5.7: Fit results for the beam-energy-constrained mass, $M_{bc} = \sqrt{E_{beam}^2 - \mathbf{p}_D^2}$, for the D^- candidates. The solid blue line represents the total fit, the solid red line represents the signal fit and the dashed blue line represents the combinatorial background.

When the first method for π^0 reconstruction is employed, the ΔE constraint is $-0.097 < \Delta E$ (GeV) < 0.047, calculated on the same way as explained for D^- It is observed that, in data, a small peak around zero appears and a large, wide peak makes an appearance at around -0.9 GeV. This can be explained by the contribution of unrelated tracks that were misidentified and included in the D^+ candidate reconstruction. Since they were not identified correctly, the D^+ energy is not around the beam energy and ΔE is not zero.

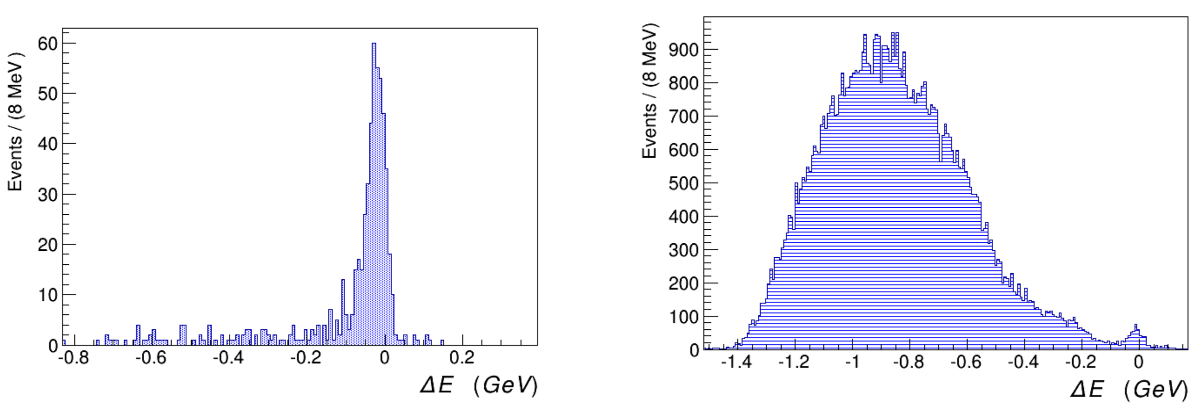

Figure 5.8: $\Delta E = E_{beam} - E_D$ for the D^+ candidates when the first method for π^0 reconstruction, π^0 invariant mass reconstruction, is considered. The left plot shows exclusive MC results, while the right one shows data.

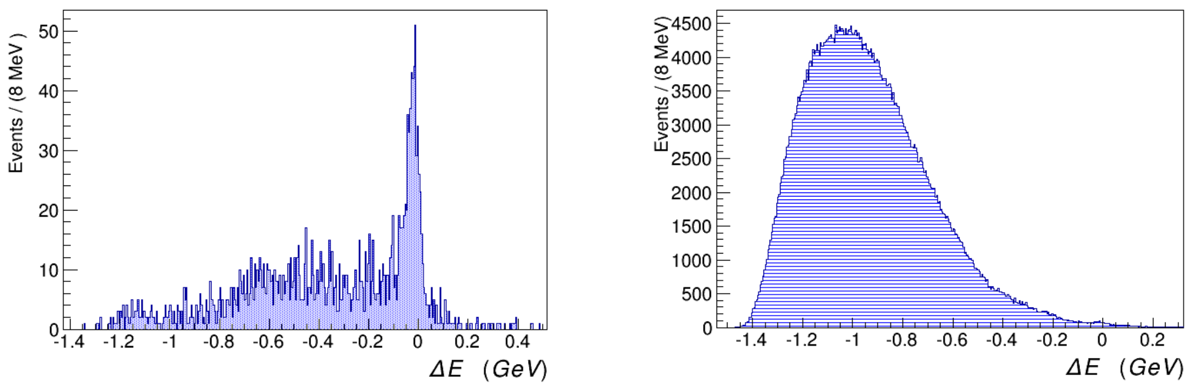

Figure 5.9: $\Delta E = E_{beam} - E_D$ for the D^+ candidates when the second method for the reconstruction of π^0, kinematic fitting, is considered. The left plot shows exclusive MC results, while the right one shows data.

Fig. 4.17 shows the ΔE curves for exclusive MC and data when kinematic fitting is used for the reconstruction of π^0. For this method, the ΔE constraint is $-0.096 < \Delta E$ (GeV) < 0.048. The expected peak around zero is almost non-existent in data, and the number of events included in the wide peak appearing around -1.1 GeV is much larger than that for the first π^0 reconstruction method. These results support the hypothesis that many tracks that are not of relevance for this process have been included in the analysis, making the results for the D^+ reconstruction via kinematic fitting of π^0 unreliable.

The beam-energy-constrained mass M_{bc} is shown in Fig. 5.10 for both π^0 reconstruction methods. Drawn in blue vertical lines is the result for when kinematic fitting is employed for the π^0 reconstruction, whereas the curve filled with red horizontal lines represents the result after π^0 invariant mass reconstruction. It is observed that when kinematic fitting is considered, the curve presents a tail on the left side that unavoidably includes background counts to the signal region. From this observed curve shape, together with the information obtained from the ΔE analysis, it is concluded that the D^+ reconstruction method in which π^0 kinematic fitting is considered is not valid for this analysis. However, the curve for when a π^0 invariant mass reconstruction is performed appears to be appropriate for further analysis. Therefore, the signal yield is obtained. The fit for that curve is shown on the right plot of Fig. 5.10. The signal shape is fit by a Crystal Ball function and the background is fit by a second-order Chebyshev polynomial function. The signal yield is 447 ± 24 events and the D^+ candidates are reconstructed with an efficiency of $(9.666 \pm 0.006)\%$. With these data, the branching fraction is calculated to be $\mathcal{B}(D^+ \to \pi^+\pi^0\pi^0) = 0.0185 \pm 0.0006$, which is about four times higher than the value published by the PDG, $(4.5 \pm 0.4) \times 10^{-3}$ [8].

The branching fraction can also be calculated from inclusive MC results. The signal yield for D^- for the inclusive MC sample is 2947980 ± 1815, while that for the D^+ candidates reconstructed via π^0 invariant mass reconstruction is 4497 ± 68. This corresponds to a branching fraction of 0.0161 ± 0.0002, which is similar to that obtained with data. The fact that this method, commonly employed by BESIII for the reconstruction of D mesons, fails to resolve the branching fraction suggests that there may be some other interfering channels in this reconstruction that do not allow a proper measurement of the correct number of D^+ for the channel of interest.

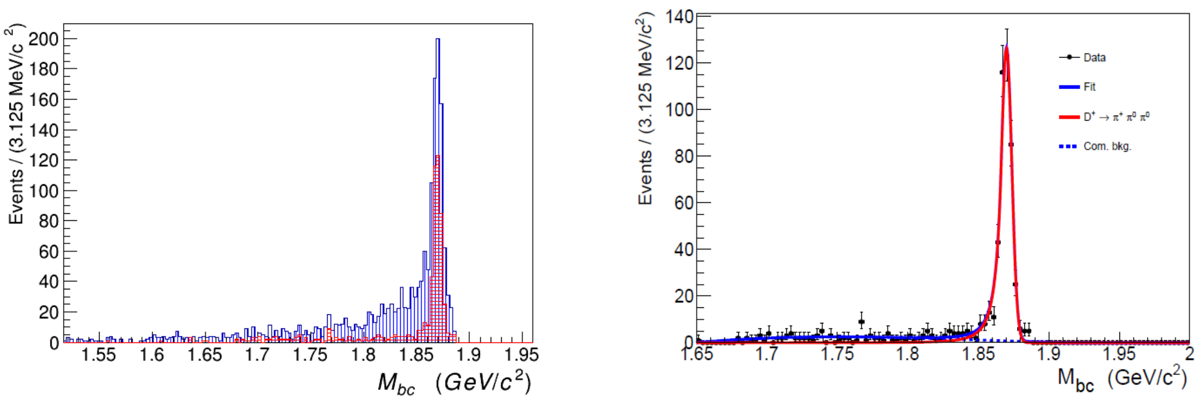

Figure 5.10: Beam-energy-constrained mass M_{bc} of the D^+ candidates. The left plot shows the M_{bc} results for the π^0 invariant mass reconstruction (red horizontal lines) and for when kinematic fitting is employed instead (blue vertical lines). the right plot shows the fit results for the first method of π^0 reconstruction (π^0 invariant mass reconstruction with two photons). The dots represent data, the solid blue line represents the total fit, the solid red line represents the signal fit and the dashed blue line stands for the combinatorial background.

5.3 Results and discussion

The branching fraction $\mathcal{B}(D^+ \to \pi^+\pi^0\pi^0)$ calculation is done by means of equation 3.1 for each of the methods exposed throughout this chapter are summarised in Table 5.1.

In this case, both methods for the reconstruction of D^+ yield results in disagreement with the PDG value, $\mathcal{B}(D^+ \to \pi^+\pi^0\pi^0) = (4.5 \pm 0.4) \times 10^{-3}$ [8]. For the invariant mass reconstruction of D mesons, kinematic fit of π^0 results in a higher efficiency on the D^+ reconstruction, and all the results are consistent between them. However, kinematic fitting of π^0 seems to not be useful when reconstruction via ΔE and M_{bc} takes place.

since the later method including kinematic fitting for π^0 was the method employed by the CLEO-c collaboration to measure $\mathcal{B}(D^+ \to \pi^+\pi^0\pi^0)$ and it is also the standard method used in

BESIII for the reconstruction of D mesons, the analysis via this method should be refined. This method provides the advantage of a better mass resolution and a cleaner combinatorial background as opposed to invariant mass reconstruction. A cut on the invariant mass of the π^0 pair proposed in [13] could be applied in order to obtain better results. Moreover, the contribution of other decay channels, such as $K_S^0 \to \pi^0\pi^0$ or $\rho^+ \to \pi^+\pi^0$, should be studied and substracted in order to improve the event selection for the reconstruction via the channel of interest.

	D^+ **inv. mass reconst.**						D^+ **reconst. via** ΔE, M_{bc}	
	No cuts in D^+		$\overrightarrow{p}$ **cut**		$\overrightarrow{p}$ **and** M **cuts**		π^0 **A**	π^0 **B**
	π^0 **A**	π^0 **B**	π^0 **A**	π^0 **B**	π^0 **A**	π^0 **B**		
$N_{sig}^{D^-}$	329868 ± 1750						254967 ± 646	
$N_{sig}^{D^+}$	329 ± 54	454 ± 75	341 ± 18	-	272 ± 16	-	447 ± 24	-
ϵ_{D^+} (%)	10.0 ± 0.3	11.7 ± 0.3	8.4 ± 0.3	13.9 ± 0.4	7.4 ± 0.2	-	9.666 ± 0.006	12.004 ± 0.006
$\mathcal{B}$ (10^{-3})	10 ± 2	12 ± 2	12.6 ± 0.8	-	11.4 ± 0.7	-	18.5 ± 0.9	-
PDG [8] $\mathcal{B}$ (10^{-3})	4.5 ± 0.4							

Table 5.1: Summary of the results $\mathcal{B}(D^+ \to \pi^+\pi^0\pi^0)$ for the analysis of 2011 data from BESIII.
π^0 **A** refers to the reconstruction of D^+ when π^0 invariant mass reconstruction is considered.
π^0 **B** refers to the reconstruction of D^+ when π^0 kinematic fitting is considered.

Chapter 6

Conclusions and outlook

Albeit the success of the Standard Model (SM) of particle physics to explain and unify two of the fundamental interactions, electromagnetism and the weak interaction, the third of the forces described by this model, the strong interaction, still presents many unanswered questions. For instance, there is not still an explanation on why the origin of hadron masses: why the mass of the particles that we observe does not correspond to the sum of its constituent quarks. The study of charmonium states can shed some light in this regard. These states lie right in between the high energy region in which perturbative methods can be employed for the study of strong interaction (corresponding to the asymptotic freedom regime for quarks) and the low energy region in which non-perturbative methods are needed (corresponding to quark confinement), making it a perfect candidate for the study of the strong interaction.

The aforementioned study can be carried out at the BESIII detector, located in Beijing, China. This detector is designed to operate in the charmonium mass region in order to perform spectroscopy of not only charmonium states but also glueballs and other exotic states. The study of charm physics is also an objective of the BESIII experiment, and it is the main interest of the work presented in this thesis. D mesons can provide valuable information about the V_{cd} and V_{cd} elements of the quark-mixing matrix and also serve as a mean to study CP-violation processes. In this work, a D meson Cabibbo-suppressed decay, $D^+ \to \pi^+\pi^0\pi^0$ is studied. Cabibbo-suppressed decays are mediated by a low probability quark-mixing matrix element. The study of this decays, together with rare and forbidden decays of D mesons, can unveil physics beyond the SM.

The aim of the study of the $D^+ \to \pi^+\pi^0\pi^0$ decay presented in this thesis revolves around the measurement of the branching fraction of the mentioned decay. The currently known value is based on a study made 11 years ago by the CLEO-c collaboration with 281 pb^{-1} of data at the center-of-mass energy of the ψ'' charmonium state, utilised for the production of D^+D^- pairs. Nevertheless, the BESIII collaboration collected the world's largest data set at that same center-of-mass energy between 2010 and 2011, 2.93 fb^{-1} of data. Thus, a precision measurement of the branching fraction $\mathcal{B}(D^+ \to \pi^+\pi^0\pi^0)$ can be executed in order to improve the current value.

In this thesis, two different methods were utilised with the aim of improving such a value: invariant mass reconstruction of the D mesons from their decay products and reconstruction their reconstruction via the use of the kinematic variables ΔE and M_{bc}. None of the methods were able to provide a clean enough event selection and, therefore, the current value for $\mathcal{B}(D^+ \to \pi^+\pi^0\pi^0)$ could not be improved within the scope of this work. Inclusive MC results were consistent with data results, which indicates that the D^+ event selection is consistent but not correct, since the value obtained for the branching fraction does not correspond to the one in the PDG, $(4.5 \pm 0.4) \times 10^{-3}$. The event selection fails to remove peaking backgrounds that are misidentified as signal events for the channel of interest.The reason behind this is that some other decay channels interfere with the decay channel of interest, like for instance $\rho^+ \to \pi^+\pi^0$, $(f_0(980) \to \pi^0\pi^0$, $K_S^0 \to \pi^0\pi^0$ and non-resonant $\pi^+\pi^0\pi^0$ contributions. A continuation of the study presented in this thesis should account for all of this sources of background in order to achieve the objective of improving the precision of $\mathcal{B}(D^+ \to \pi^+\pi^0\pi^0)$. Moreover, additional channels for the reconstruction of D^- should be included in a further analysis in order to increment about 10 times the statistics available for the calculations.

Once the suppression of interfering background and the refinement of the reconstruction algorithm are implemented, the calculation of the systematic errors involved in the analysis needs to be performed. Some examples of sources of systematic error involved in this analysis are: fitting errors, errors in the determination of the background, the restriction on the number of stored photons and charged particles per event, cuts on the reconstruction of the $D^\pm$ mesons and errors involved in the kinematic fitting of π^0. An extensive analysis of the contribution of all of these sources plus others that have not been mentioned is needed.

Subsequently, Dalitz analysis of the $D^+ \to \pi^+\pi^0\pi^0$ decay can be performed for the first time with the BESIII data samples. The four dominant contributions mentioned earlier can be included:

1. ρ^+, with $\pi^0\rho^+$ $(\rho^+ \to \pi^+\pi^0 \sim 100\%)$
2. $f_0(980)$, with $\pi^+ f_0(980)$ $(f_0(980) \to \pi^0\pi^0 \sim 100\%)$
3. K_S^0, with $\pi^0\pi^0$ $(K_S^0 \to \pi^0\pi^0 \sim 30\%)$
4. Non-resonant $\pi^+\pi^0\pi^0$ contributions

The involvement of $K_S^0 \to \pi^0\pi^0$ can also be of use for the calculation of the branching fraction $\mathcal{B}(D^+ \to \pi^+ K_S^0)$ via the decay $K_S^0 \to \pi^0\pi^0$. The current value, $\mathcal{B}(D^+ \to \pi^+ K_S^0) = (1.47 \pm 0.08)\%$ [8], was determined via $K_S^0 \to \pi^+\pi^-$ by the E687 Collaboration at Fermilab in 1995 [38]. The BESIII data samples could be utilised to improve its measurement via the later method, but they also offer the possibility of doing it via the $K_S^0 \to \pi^0\pi^0$ method as an independent measurement.

In conclusion, the study presented on this thesis can be extended in several directions. Studying charmed meson decays covers several areas of interest for physics, ranging from information about the CKM angle γ/ϕ_3 to $D^0 - \overline{D^0}$ mixing, CP violation and, in this case, Cabibbo-suppressed decays; making charmed states an interesting field of research.

Bibliography

[1] G. Aad *et al.* (ATLAS Collaboration), Phys. Lett. B **716**, 1 (2012), `arXiv:1207.7214 [hep-ex]`

[2] S. Chatrchyan *et al.* (CMS Collaboration), Phys. Rev. Lett. B **716**, 30 (2012), `arXiv:1207.7235`

[3] R. Aaji *et al.* (LHCb Collaboration), Phys. Rev. D **95**, 012002 (2017), `arXiv:1606.07898 [hep-ex]`

[4] CERN website, `http://home.web.cern.ch/`

[5] J. Messchendorp (BESIII Collaboration), PoS Bormio2013 043 (2013), `arXiv:1306.6611 [hep-ex]`

[6] BESIII Collaboration, `http://bes3.ihep.ac.cn/`

[7] PANDA Collaboration, `http://www-panda.gsi.de/`

[8] C. Patrignani *et al.* (Particle Data Group), Chin. Phys. C **40**, 100001 (2016) and 2017 update.

[9] LHCb website, `http://lhcb.web.cern.ch/lhcb/`

[10] P. Harrison and H. R. Quinn (BaBar Collaboration), SLAC-R-504 (1998).

[11] A. Abashian *et al.* (Belle Collaboration), Nucl. Instr. and Meth. in Phys. Research A **479**, 177 (2002).

[12] Y. Kubota *et al.*, Nucl. Instr. and Meth. in Phys. Research A **320**, 66 (1992).

[13] P. Rubin *et al.*, (CLEO Collaboration), Phys. Rev. Lett. **96**, 081802 (2006), `arXiv:hep-ex/0512063`

[14] M. Ablikim *et al.* (BESIII Collaboration), Chin. Phys. C **37**, 123001 (2013), `arXiv:1307.2022`

[15] M. Asner *et al.* (BESIII Collaboration), Int. J. Mod. Phys. A **24** (2009), `arXiv: 0809.1869.`

[16] T. Appelquist and H. D. Politzer, Phys. Rev. Lett. **34**, 43 (1975),

doi:10.1103/PhysRevLett.34.43

[17] M. Ablikim *et al.*, Phys. Lett. B **659**, 74 (2008), doi:10.1016/j.physletb.2007.11.078

[18] D. Besson *et al.* (CLEO Collaboration), Phys. Rev. Lett. **104**, 159901 (2010).

[19] S. Choi *et al.* (Belle Collaboration), Phys. Rev. Lett. **91**, 262001 (2003), arXiv:hep-ex/03090320

[20] B. Aubert *et al.* (BaBar Collaboration), Phys. Rev. Lett. **95**, 142001 (2005), arXiv:hep-ex/0506081

[21] M. Ablikim *et al.* (BESIII Collaboration), Phys. Rev. Lett. **110**, 252001 (2013), arXiv:1303.5949

[22] S. Malde *et al.* (LHCb Collaboration), (2016), http://cds.cern.ch/record/2223391

[23] M. Ablikim *et al.* (BESIII Collaboration), Phys. Rev. D **90**, 012001 (2014), arXiv:1405.1076.

[24] BESIII Collaboration, Nucl. Instrum. and Meth. Phys. Res. A **598**, 7 (2009), doi:10.1016/j.nima.2008.08.072

[25] M. Ablikim *et al.* (BESIII Collaboration), Nucl. Instrum. and Meth. Phys. Res. A **614**, 345 (2010), doi:10.1016/j.nima.2009.12.050

[26] W. Li *et al.*, Proceedings of CHEP (2006),

[27] CERNLIB - The CERN Program Library, http://cernlib.web.cern.ch/cernlib/.

[28] CLHEP - A Class Library for High Energy Physics, http://proj-clhep.web.cern.ch/proj-clhep.

[29] R. Brun and F. Rademakers, Nucl. Instrum. and Meth. Phys. Res. A **389**, 81 (1997), doi:10.1016/S0168-9002(97)00048-X

[30] S. Agostinelli *et al.*, Nucl. Instrum. and Meth. Phys. Res. A **506**, 250 (2003), doi:10.1016/S0168-9002(03)01368-8

[31] D. Zi-Yan *et al.*, Chin. Phys. C **30**, 371 (2006).

[32] R.-G. Ping, Chin. Phys. C **32**, 599 (2008), http://stacks.iop.org/1674-1137/32/i=8/a=001

[33] S. Jadach, D. F. L. Ward, and Z. Was, Comp. Phys. Comm. **130**, 260 (2000), arXiv:hep-ph/9912214

[34] A. Ryd *et al.*, http://robbep.home.cern.ch/robbep/EvtGen/GuideEvtGen.pdf

[35] J. Bian *et al.*, BESIII Analysis Note (non-published).

[36] E. D. Bloom and C. W. Peck, Annual Review of Nuclear and Particle Science **33**, 143 (1983).

[37] Q. He *et al.* (CLEO Collaboration), Phys. Rev. Lett. **95**, 121801 (2005).

[38] P.L. Frabetti *et al.* (E687 Collaboration), Phys. Lett. B **346**, 199-202 (1995).

Acronyms

ATLAS	A Toroidal LHC Apparatus
BaBar	B-Bar detector
Belle	B detector
BESIII	BEijing Spectrometer III
BEPC	Beijing Electron-Positron Collider
BOOST	BESIII Object Oriented Simulation Tool
BOSS	BESIII Offline Software System
CERN	Conseil Européen pour la Recherche Nucléaire
CKM	Cabibbo-Kobayashi-Maskawa
CLEO	particle detector at the Cornell Electron Storage Ring
CLEO-c	particle detector for charm at the Cornell Electron Storage Ring
CMS	Compact Muon Solenoid
DST	Data-Summary-Type
EMC	ElectroMagnetic Calorimeter
FSR	Final State Radiation
IHEP	Institute of High Energy Physics
ISR	Initial State Radiation
LHC	Large Hadron Collider
LHCb	Large Hadron Collider beauty
MC	Monte Carlo
MD	Muon Detector
MDC	Multilayer Drift Chamber

OZI Okubo-Zweig-Iikuza

PID Particle IDentification

PDF Probability Density Function

PDG Particle Data Group

QCD Quantum ChromoDynamics

QED Quantum ElectroDynamics

SLAC Stanford Linear Accelerator Center

SM Standard Model

TOF Time-Of-Flight